CHAPTER-3
RESULTS AND DISSCUSION

3.1 Nicotinonitriles as corrosion inhibitors

The Pyridines and their analogues are the most important class of N-heterocyclic compounds having various pharmaceutical properties such as anti-microbial, anti-viral, anti-oxidant, anti-diabetic, anti-cancer, anti-inflammatory, anti-malarial, analgesics properties [Altaf *et al* .(2015)].

The literature survey reveals that, earlier some pyridine derivatives have been reported as good corrosion inhibitors, for example, Kosari *et al.* have reported two pyridine derivatives pyridine-2 thiol (P2T) and 2-Pyridyl disulfide (2PD) as corrosion inhibitors for mild steel in 0.1 M HCl, showing 98.3% and 98.1% inhibition efficiency at 200 ppm [Kosari *et al.* (2014)]. Ansari *et al.* tested three pyridine derivatives namely 2-amino-6-methoxy-4-(4-methoxylphenyl) pyridine-3,5-dicarbonitrile (PC-1), 2-amino-6-methoxy-4-(4-methylphenyl) pyridine-3,5-dicarbonitrile (PC-2) and 2-amino-6-methoxy-4-phenylpyridine-3,5-dicarbonitrile (PC-3) for mild steel in 1 M HCl, which gave 97.4%, 95.7% and 88.0% inhibition efficiency at 400 mg/l [Ansari *et al.* (2015)]. The corrosion inhibition performance of 2-amino-4-methylpyridine (AMP) has been investigated by Mert *et al.* showed 93.9% inhibition efficiency at 50 mM for mild steel in 0.5 M HCl [Mert *et al.* (2014)].

In the present work we have investigated two pyrimidine derivatives namely as: 2-amino-6-phenyl-4-(p-tolyl) nicotinonitriles (ATN) and 2-amino-4-(4-methoxyphenyl)-6-phenylnicotinonitrile (AMN) as corrosion inhibitors for mild steel (MS) in 1 M HCl by using weight loss, electrochemical impedance spectroscopy (EIS) and potentiodynamic polarization techniques. The selection of these pyridine derivatives is

based on following considerations: (i) they contain electron rich hetero atoms (N and O), π electrons inside their skeleton through which they are likely to adsorb easily on the MS surface (ii) $-CH_3$, $-OCH_3$ electron donating groups facilitate adsorption of the molecules on MS surface. The surface analyses for MS in the absence and presence of inhibitors were carried out using scanning electron microscopy (SEM) and atomic force microscopy (AFM). The computational studies were carried out to establish the correlation between theoretical and experimental results.

3.1.1 Weight loss measurements

3.1.1.1 Effect of inhibitor concentrations

The weight loss measurement is an important technique to optimize inhibitors concentration and to find the inhibition efficiency. The weight loss results for MS in the absence and presence of ATN and AMN are listed in Table 3.1.1.

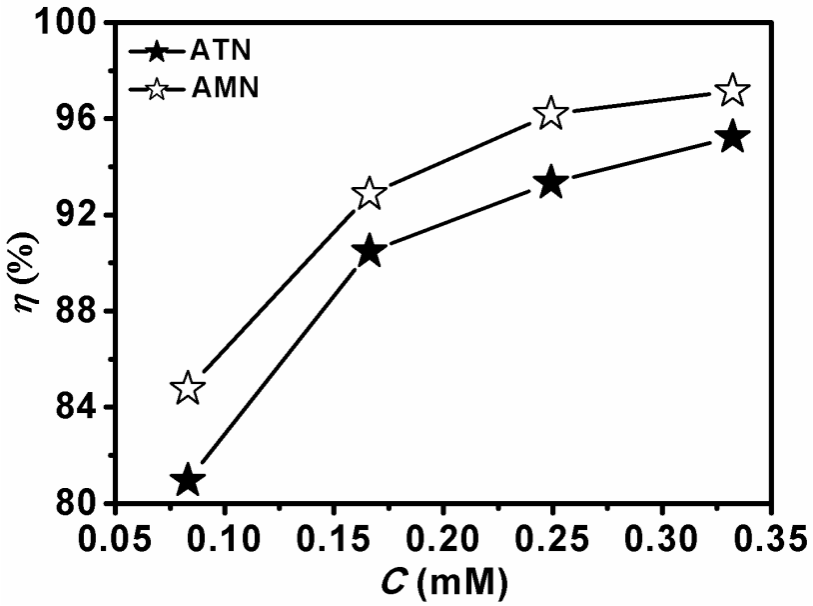

Figure 3.1.1 Effect of different concentrations of ATN and AMN on corrosion inhibition efficiency for MS in 1 M HCl.

It can be seen from the Figure 3.1.1, that the corrosion inhibition efficiency increases (80-97%) with increasing the ATN and AMN concentrations (0.08 to 0.33 mM), which indicates that the corrosion inhibition efficiency depends upon the inhibitor concentration. But, after the optimum concentration (0.33 mM) no significant changes were observed in the corrosion inhibition efficiency. The maximum inhibition efficiency obtained for ATN and AMN is 95.23% and 97.14% respectively at 0.33 mM. The increase in the inhibitor concentration causes increase in the extent of adsorption and surface coverage due to the availability of larger number of inhibitor molecules accordingly; this increases the inhibition efficiency [Verma *et al.* (2015) (a)].

Table 3.1.1 Weight loss measurements for MS in absence and presence of ATN and AMN in 1 M HCl at 308 K.

Inhibitors	**Concentrations (mM)**	**Corrosion rate (mm/y)**	**Surface coverage (θ)**	**η%**
Blank	0.0	77.9	-	-
ATN	0.08	14.8	0.80	80.95
	0.16	7.4	0.90	90.47
	0.24	5.1	0.93	93.33
	0.33	3.7	0.95	95.23
AMN	0.08	11.8	0.84	84.76
	0.16	5.5	0.92	92.85
	0.24	2.9	0.96	96.19
	0.33	2.2	0.97	97.14

The difference in corrosion inhibition efficiency of ATN and AMN is attributed to the presence of substituent groups $-CH_3$, $-OCH_3$ attached at the para position of the phenyl ring. AMN is better inhibitor than ATN due to the better electron donor group $-OCH_3$ as compared to $-CH_3$ group [Wade (2006)].

3.1.1.2 Effect of Temperature

The temperature effect (308-338 K) has been studied on MS in the absence and presence of ATN and AMN at optimum concentration, shown in Figure 3.1.2. The inhibition efficiency decreases and corrosion rate increases with increase in the temperature in both the conditions i.e. inhibitor free and inhibited solution. This can be attributed to the desorption of adsorbed inhibitor molecules from the MS surface, which exposes a greater surface area of steel in contact with the HCl, resulting in increase in corrosion rate [Ansari and Quraishi (2014)].

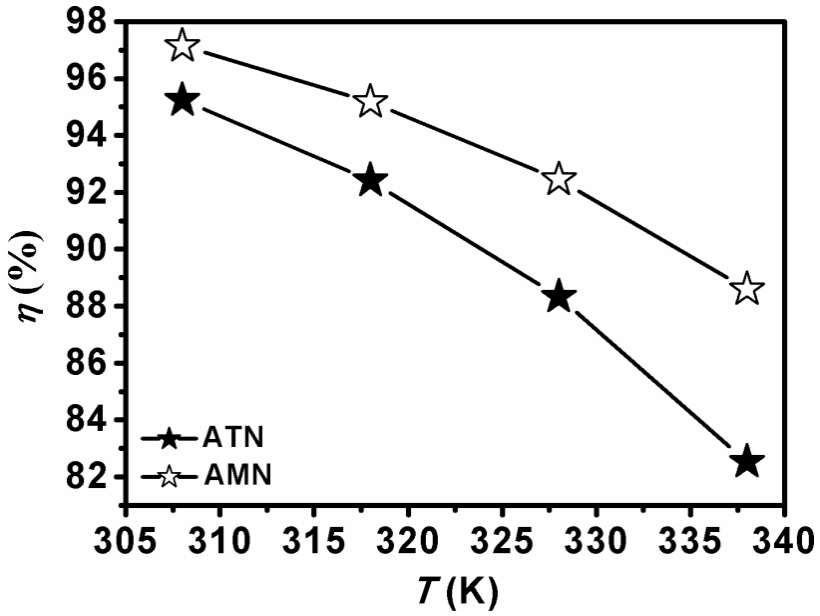

Figure 3.1.2 Effect of temperature (308-338 K) on corrosion inhibition efficiency for MS in presence of ATN and AMN in 1 M HCl.

3.1.1.3 Adsorption isotherm

It is well documented that organic compounds inhibit corrosion by adsorption mechanism [Chaitra *et al.* (2016)]. In order to understand the adsorption behaviour, appropriate adsorption isotherm was tested [Sasikumar *et al.* (2015)], [Umoren *et al.* (2014)]. The Langmuir adsorption isotherm was found to be the best fitted isotherm shown in Figure 3.1.3, with regression coefficient (R^2) values near to one.

It is reported that, the values of ΔG_{ads} varying between -40 kJ mol^{-1} or more negative suggests that the adsorption is chemisorption, while a value of ΔG_{ads} around -20 kJ mol^{-1} or less negative implies that the adsorption is electrostatic interaction i.e. physisorption. The values reported in Table 3.1.2 range between -38.45 to -39.54 kJ mol^{-1} which is close to -40 kJ mol^{-1} thereby, suggesting mixed mode of adsorption and predominantly by chemisorption [Solmaz (2014) (a)], [Solmaz (2014) (b)]

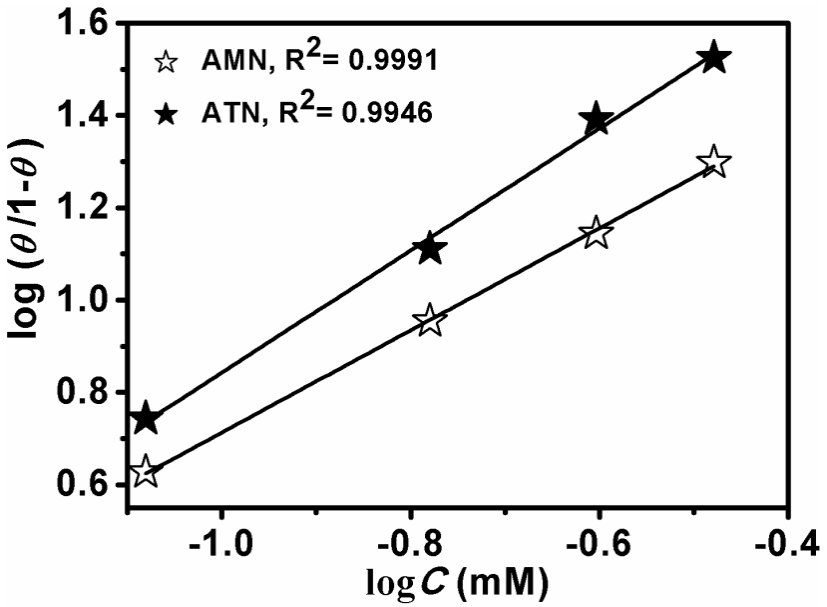

Figure 3.1.3 Langmuir adsorption isotherm plot for MS in presence of ATN and AMN.

Table 3.1.2 ΔG_{ads} at optimum concentration (0.33 mM) of ATN and AMN for MS in 1 M HCl at 308-338 K.

Inhibitors	Temperature	ΔG_{ads} (kJ mol^{-1})
ATN	308	-38.45
	318	-38.41
	328	-38.31
	338	-38.16
AMN	308	-39.79
	318	-39.64
	328	-39.61
	338	-39.54

3.1.2 Electrochemical measurements

3.1.2.1 Electrochemical impedance spectroscopy

The EIS measurement was carried out to understand the kinetics of the electrochemical process at MS/solution interface in the absence and presence of inhibitors. The Nyquist plots, equivalent circuit model and Bode-phase angle plots are presented in Figures 3.1.4 (a, b, c) and the corresponding parameters are listed in Table 3.1.3

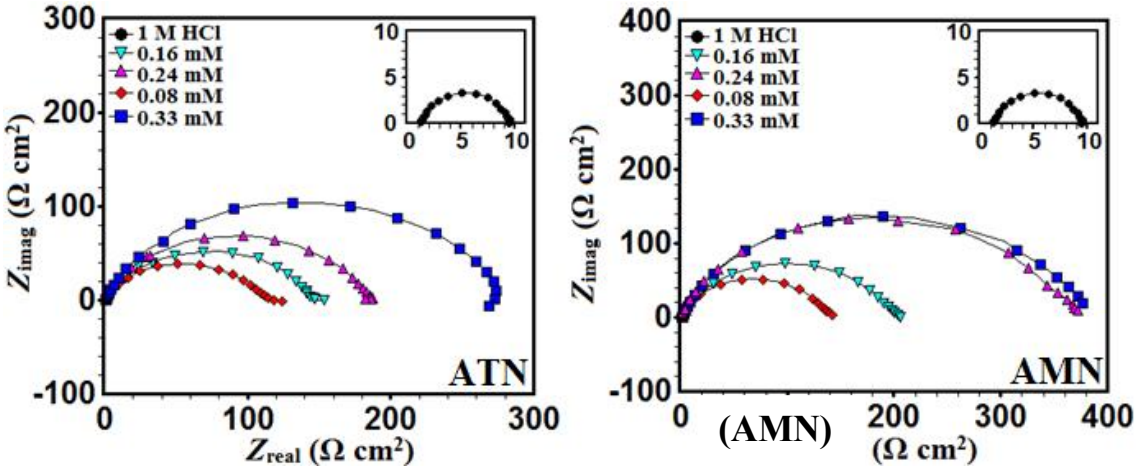

Figure 3.1.4 (a) Nyquist plots for MS in 1 M HCl without and with ATN and AMN.

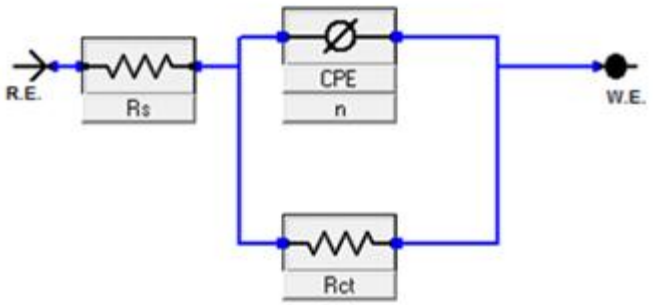

Figure 3.1.4 (b) Equivalent circuit model used to analyze the EIS data.

The obtained Nyquist plots for MS in blank as well as in inhibited solution exhibited one semicircle capacitive loop in high frequency range. This behaviour suggests that the corrosion process of MS is controlled by charge transfer process [Sudheer and Quraishi (2014)]. The obtained loops show imperfect semicircle, depressed with a centre under real axis. This kind of imperfection is attributed to the rough surface, frequency dispersion, relaxation and porosity in mass transport effects [Yadav *et al.* (2015)]. For this reason, a constant phase element (CPE) has been introduced to the equivalent circuit model for the accurate fit, which is used to analyse the Nyquist loops [Amin *et al.* (2009)]. The diameter of the semicircle loop increases with increase in the concentrations of ATN and AMN. The diameter of the Nyquist loops corresponds to charge transfer resistance (R_{ct}), which can be determined from the difference in the real impedance at lower and higher frequencies. It can be observed that the R_{ct} values increase with increasing concentrations of ATN and AMN and the highest R_{ct} value was obtained for AMN i.e., 374.81 Ω cm^2 at 0.33 mM. The maximum inhibition efficiency obtained for ATN and AMN are 96.67% and 97.59% respectively at 0.33 mM. It can also be clearly seen that from the results that with increase in the R_{ct} values, decrease in double layer capacitance (C_{dl}) is observed [Dandia *et al.* (2013)]. This is attributed to a decrease in the dielectric constant, or increase in the double-layer thickness because of adsorption of inhibitor molecules on MS surface to protect metal from acid attack.

The ideal capacitive behaviour for Bode and phase angle would result, if the slope value attains -1 and phase angle value attains -90° at the intermediate frequencies. In the presence of ATN and AMN as shown in Figure 3.1.4 (c), the respective values of the slope and phase angle range from 0.71 to 0.78, and 60° to 73° as compared to those of the blank solution i.e. 0.53 and 40° respectively reported in Table 3.1.3, suggesting the

formation of pseudo-capacitive film on the MS surface and an indication of the inhibition of MS corrosion in 1 M HCl [Singh *et al.* (2015)].

Table 3.1.3 Electrochemical impedance parameters for MS in absence and presence of ATN and AMN in 1 M HCl.

Inhibitors	**Concentrations (mM)**	R_{ct} **(Ω cm^2)**	C_{dl} **(μFcm^{-2})**	η**%**	$-S$	$-\alpha°$
Blank	0.0	9.0	106	-	0.53	40.40
ATN	0.08	110.82	80	91.87	0.74	63.22
	0.16	144.58	78	93.77	0.71	60.62
	0.24	188.37	57	95.22	0.78	68.01
	0.33	273.34	50	96.70	0.78	68.97
AMN	0.08	142.63	74	93.69	0.77	63.00
	0.16	198.91	72	95.47	0.74	66.79
	0.24	374.06	42	97.59	0.77	69.39
	0.33	374.81	30	97.59	0.76	73.90

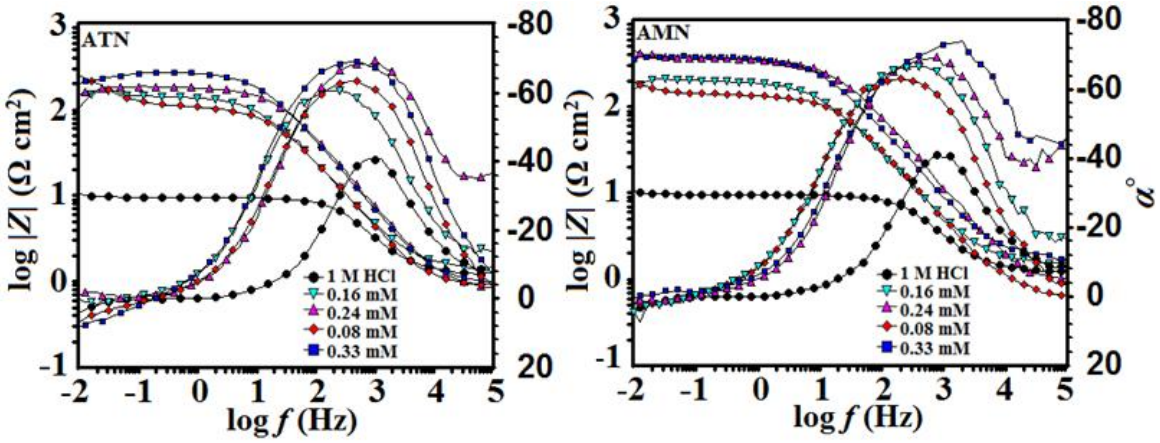

Figure 3.1.4 (c) Bode (log *f* vs log |*Z*|) and phase angle (log *f* vs α) plots for MS in 1 M HCl without and with ATN and AMN.

3.1.2.2 Potentiodynamic polarization measurements

The Tafel curves obtained for MS in the absence and presence of ATN and AMN are shown in Figure 3.1.5 and related parameters such as corrosion potential, E_{corr} corrosion current density, i_{corr} are listed in Table 3.1.4.

Table 3.1.4 Polarization parameters for MS in absence and presence of ATN and AMN in 1 M HCl.

Inhibitors	Concentrations (mM)	i_{corr} (μAcm-^{2})	E_{corr} (mV/SCE)	η%
Blank	0.0	1390	-445	-
ATN	0.08	215	-564	84.53
	0.16	174	-548	87.48
	0.24	141	-589	89.85
	0.33	37.8	-568	97.28
AMN	0.08	106	-526	92.37
	0.16	102	-511	92.66
	0.24	101	-562	92.73
	0.33	28.7	-556	97.93

The i_{corr} value for MS in 1 M HCl is 1390 μAcm^{-2} and for the ATN and AMN are 37.8 μAcm^{-2} and 28.7 μAcm^{-2} at 0.33 mM respectively. The decrease in the i_{corr} values suggests that the presence of nicotinonitriles retarded the electrochemical reaction on MS surface. This is due to the formation of protective film on MS surface [ji *et al.* (2011)], [Ebenso *et al.* (2012)].

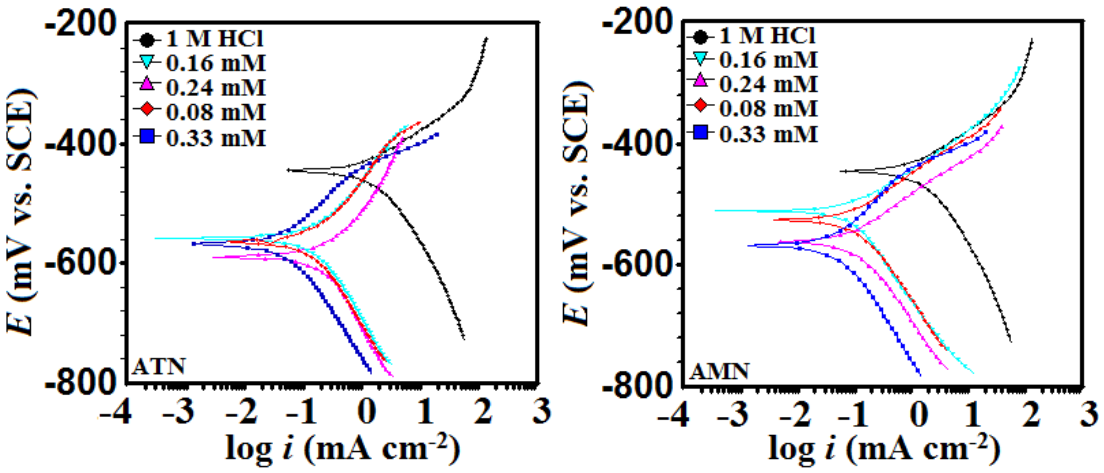

Figure 3.1.5 Polarization curves for MS in 1 M HCl without and with ATN and AMN.

3.1.3 Surface characterization

The SEM micrographs of MS in absence and presence of ATN and AMN are shown in Figure 3.1.6 (a-c). Figure 3.1.6 (a) shows the MS sample immersed in acid solution without inhibitor. In that micrograph, the MS surface is damaged due to acid attack. The micrographs of MS treated with inhibitors are shown in Figure. 3.1.6 (b, c) are smooth and protected due to adsorption of inhibitor molecules on the MS surface.

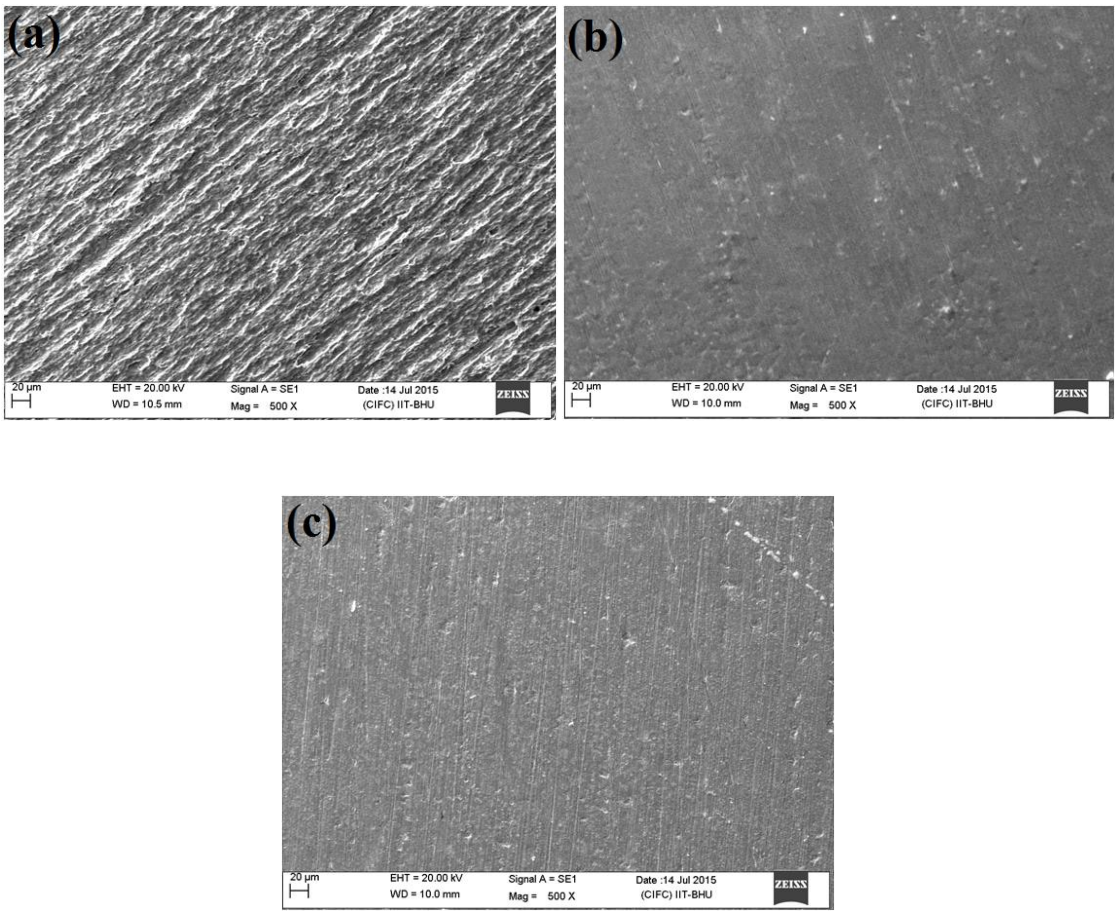

Figure 3.1.6 (a-c) SEM micrographs (a) in 1 M HCl and (b, c) in presence of ATN and AMN at 0.33 mM.

In addition to the surface study, the AFM analysis is also a useful technique. In the absence of nicotinonitriles the surface displayed an extremely rough topography due to unhindered corrosion attack (Figure 3.1.7 (a)) while in the presence of nicotinonitriles, the MS shows a smoother surface (Figure 3.1.7 (b, c)).

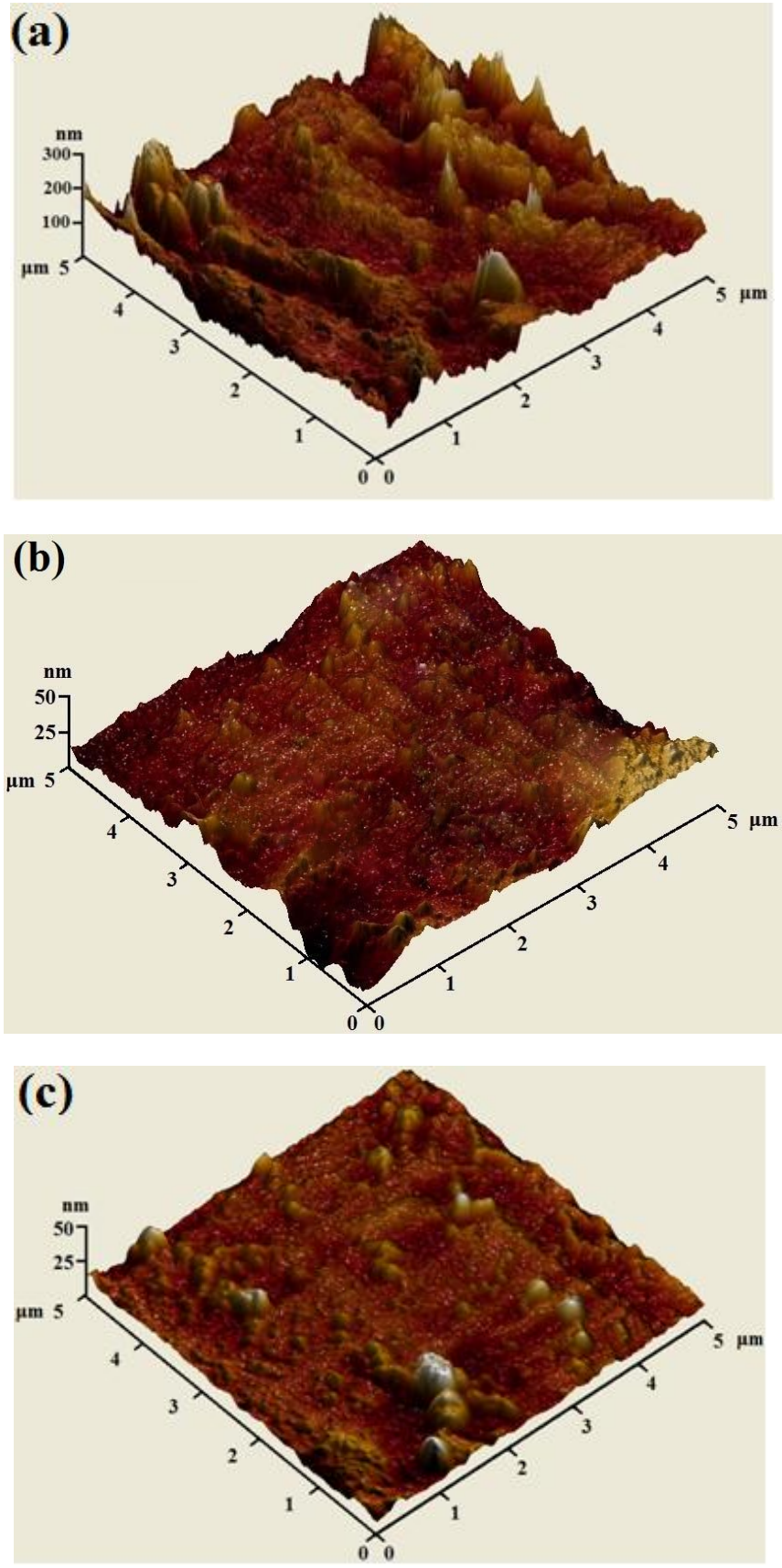

Figure 3.1.7 (a-c) AFM micrographs of MS surface (a) in 1 M HCl and (b, c) in presence of ATN and AMN at 0.33 mM.

Both the surface analysis techniques suggest that the addition of the ATN and AMN inhibit the corrosion of MS, as depicted by the micrographs in which the roughness of the surface is very less as compared to the acid treated metal surface [Murulana *et al.* (2012)].

3.1.4 Quantum chemical calculations

The quantum chemical (QC) studies have been used to understand the effect of nicotinonitriles molecular structures (ATN and AMN) on inhibition efficiency. First of all the structures of the ATN and AMN molecules were optimized according to the total energy minimization. The obtained geometries of both molecules in gas phase are presented in Figure 3.1.8.

The skeletons of both molecules are planar except substituted phenyl (III) ring which is slightly twisted compared to the remaining part of the molecules. The near planar geometries of these compounds might contribute to their high inhibition efficiencies because; high degree of planarity had been reported to favour optimum adsorption of inhibitor molecules on metal surface leading to enhanced inhibition efficiency. The angle of rotation of the molecule AMN is smaller than the twist angle of the molecules ATN. It explains the experimentally proved higher inhibition efficiency of the AMN molecule than the ATN one. The parameters obtained from QC, based on the difference in their molecular electronic structure, both in the gas phase (neutral and protonated) are listed in Table 3.1.5.

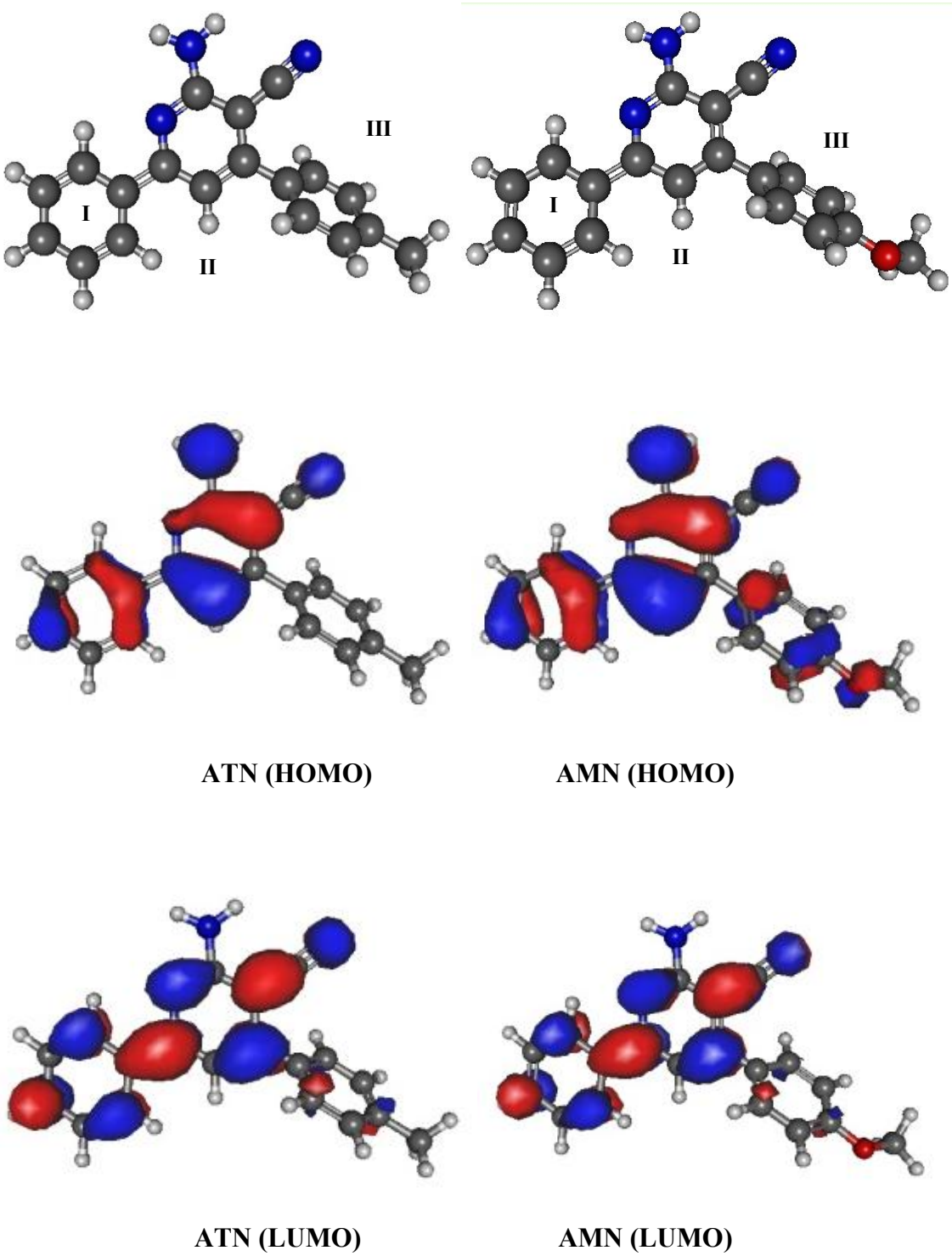

Figure 3.1.8 The optimized molecular structures, HOMO and LUMO orbitals distribution of ATN and AMN in gas phase.

Table 3.1.5 Quantum chemical parameters derived from the B3LYP/6-311++G** method of the studied ATN and AMN.

Parameters→ Compounds↓	E_{HOMO} **(eV)**	E_{LUMO} **(eV)**	ΔE **(eV)**	χ **(eV)**
Neutral molecule in Vacuo				
ATN	-6.16	-1.94	4.22	4.05
AMN	-6.12	-1.91	4.21	4.02
Protonated molecule in Vacuo				
ATN	-9.79	-6.10	3.69	7.95
AMN	-9.74	-5.73	4.01	7.74

The HOMO electron density surface provides information about the sites of the molecule that are most likely to donate electrons to the appropriate orbital of an acceptor species, while the LUMO electron density surface suggests the sites of the molecule that possess higher chances of accepting electrons from a donor species [Obot *et al.* (2015)]. The orbital representation of the studied compounds exhibited in Figure 3.1.8 shows similar features of the LUMO for both nicotinonitriles but clearly different HOMOs are observed. For this reason, the variation in the inhibition efficiencies of the studied molecules might not be describable based on the LUMOs. Both the HOMOs and the LUMOs of the studied molecules comprise the π type orbitals, which suggest that the molecules can favourably interact with the vacant/filled d- or p- orbitals of the metal atom. The HOMO of ATN is widely distributed over all the rings in the molecule except the phenyl (III) ring, which does not contribute to the HOMO. On other hand, the HOMO of AMN is well delocalized over whole system including phenyl (III).

The effects of the methyl and methoxy substituents present in ATN and AMN respectively are very apparent in the HOMO orbital distributions. Higher value of E_{HOMO}, indicates that the molecule has a higher capability to give electrons to the required acceptor molecules having the low energy empty molecular orbital [Madkour and Elroby (2015)], whereas lower value of E_{LUMO} suggests that the molecule easily accepts electrons from the donor molecule [Olasunkanmi *et al.* (2015)]. The E_{HOMO} values obtained of the studied neutral and protonated compounds in the gas phases are in the order: AMN > ATN, which agrees with the order of the experimental inhibition efficiencies. The energy gap, ΔE is another index of the molecular reactivity. Molecules with lower ΔE are usually more reactive and possess higher inhibition efficiency [Olasunkanmi *et al.* (2015)]. The changes of the ΔE values obtained for the studied compounds in neutral and protonated state show different trends. The trend of ΔE obtained for ATN and AMN molecules in neutral medium correlates with experimental results but in the case of protonated molecules the obtained results are not in agreement with the experimental inhibition efficiencies. This is not unexpected because in the protonated form the E_{LUMO} values of ATN and AMN show slightly different trend. The global electronegativity, χ is another reactivity index that predicts the extent to which a molecule retains its electrons.

Increase in the χ means the fall of the chance of electron donation by the molecule and vice versa [Musa *et al.* (2012)]. The trends of the χ values obtained for the studied compounds shown in Table 3.1.5 are ATN>AMN, which suggest that AMN has higher possibility to donate electrons to an electrophilic centre such as the iron surface populated by positive charges. The electron-donating effects of $–OCH_3$ and $–CH_3$ are well known [Wade (2006)], and the established trend of electron-donating abilities of the groups present in the studied compounds is $–OCH_3$ (in AMN) > $-CH_3$ (in ATN).

So, the inhibition trend obtained by the experimental study AMN>ATN is also supported by theoretical approach.

3.1.5 Monte Carlo simulation

The Monte Carlo simulation (MC) helps to understand the interaction between the inhibitor molecules and metal surface. It helps to predict the most stable adsorption sites on metal surface. The calculated outputs from MC simulation are listed in Table 3.1.6 and the most stable low energy adsorption configurations of ATN and AMN on Fe (110) surface are shown in Figure 3.1.9.

Table 3.1.6 Average adsorption energy of the ATN and AMN molecules at the Fe (110) surface and the average total energy of the investigated systems.

Systems Energy	Total Energy (kcal mol^{-1})	Adsorption (kcal mol^{-1})
Neutral molecule in Vacuo		
Fe (110) + ATN	-25.85	-17.73
Fe(110) + AMN	-36.25	-21.31
Protonated molecule in Vacuo		
Fe (110) + ATN	-31.56	-17.57
Fe(110) + AMN	-43.47	-20.31

The conformational arrangement of the ATN and AMN molecules at the surface of Fe (110) prefer the planar configuration of the inhibitors to the surface of iron. The distance between inhibitors and the surface of Fe is in the range of 0.3 to 0.4 nm for both investigated systems.

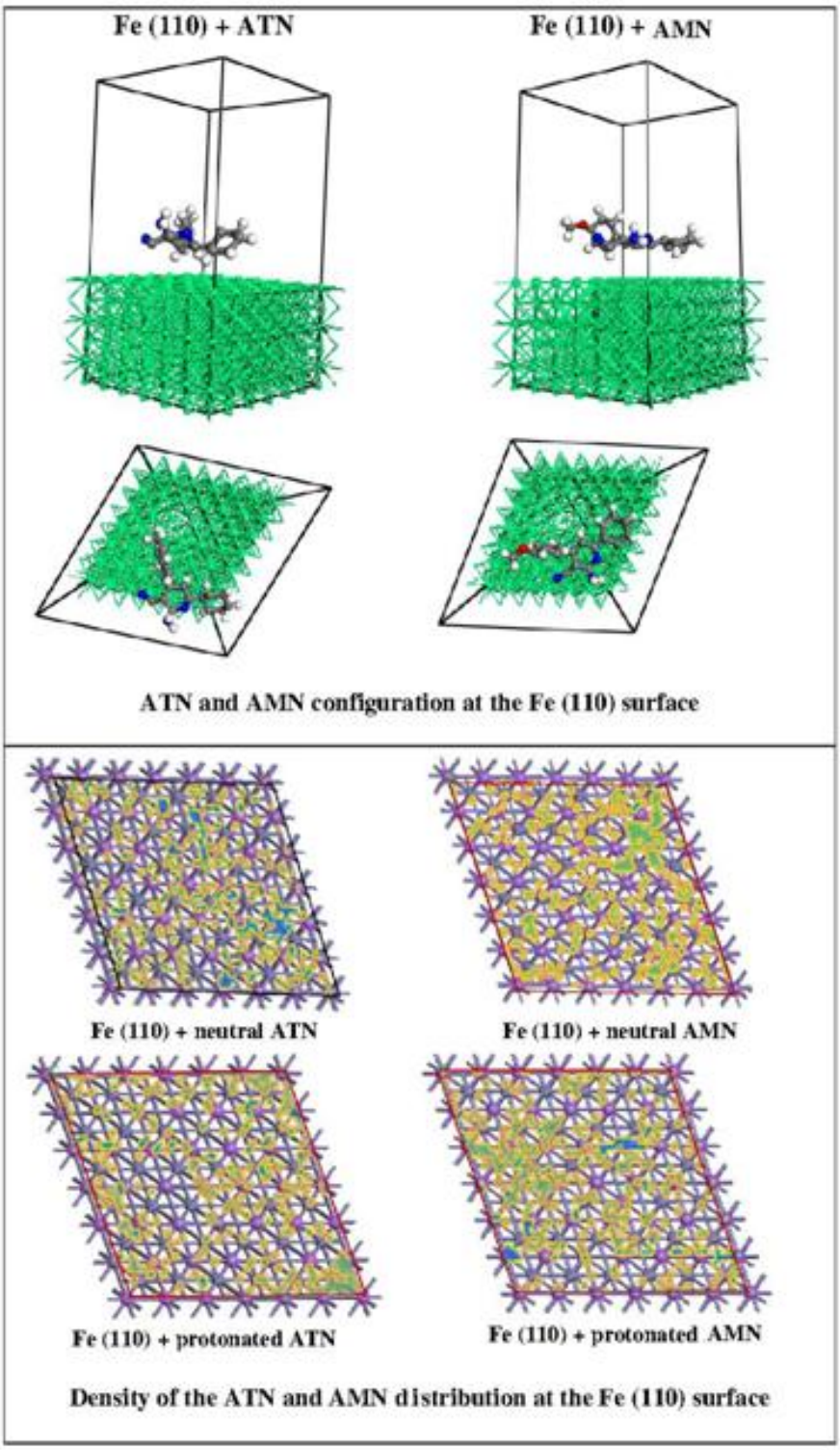

Figure 3.1.9 Side and top views of the most stable low energy configuration for the adsorption of ATN and AMN on Fe (110) surface obtained by Monte Carlo Simulations and the density of the inhibitors distribution at the surface of iron.

At the bottom of Figure 3.1.9 the density of the ATN and AMN adsorption at the surface of Fe (110) is presented. One can see that the inhibitors do not prefer any special places at the iron surface. The presented surface is homogenously covered by the isodensity shapes. This homogeneous distribution is caused by the lack of atomic terraces and dense packing of atoms on the studied surface.

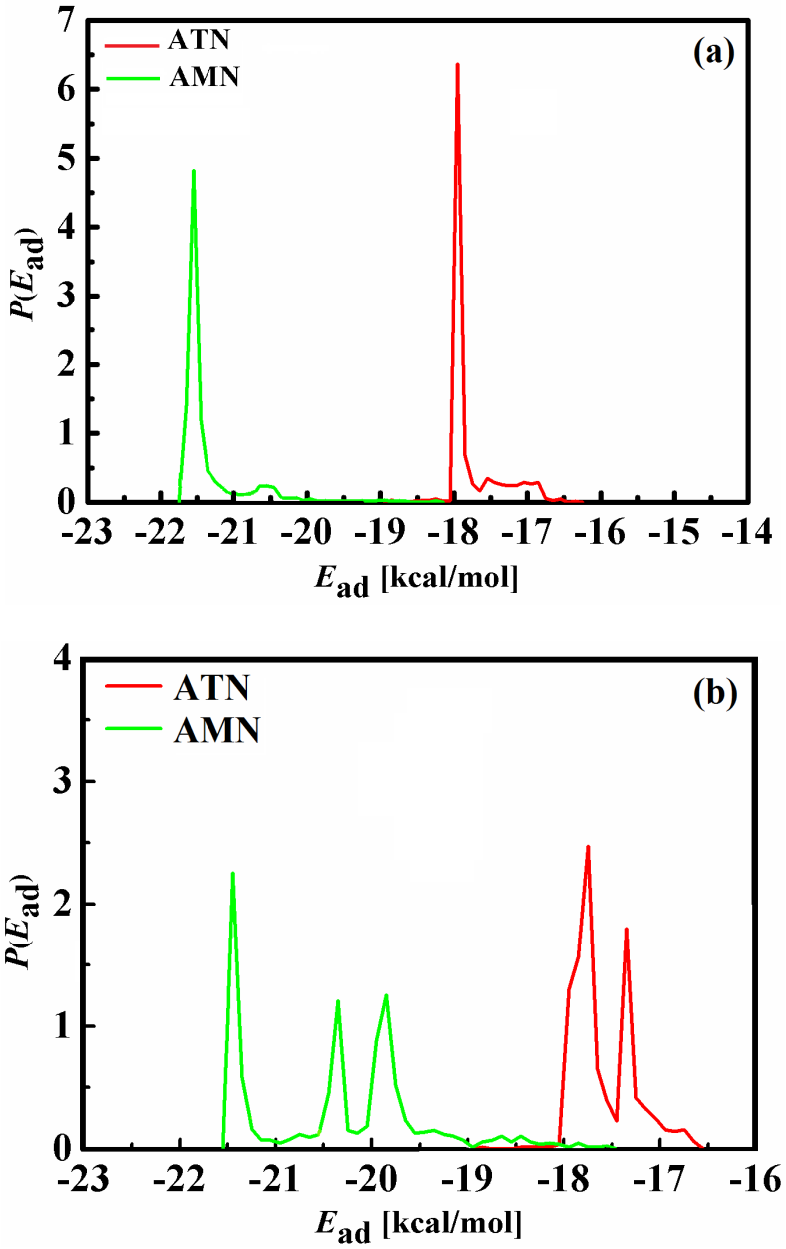

Figure 3.1.10 The adsorption energy distribution of the adsorbate (ATN and AMN molecules) on Fe (110) surface for (a) non-protonated and (b) protonated molecules.

The adsorption energy distribution presented in Figure 3.1.10 for neutral and protonated molecules show one pronounced peak in each investigated regimes. It means that the AMN and ATN molecules stick to the surface of iron in one configuration; they are always planar to the Fe (110) surface.

The adsorption energy is attributed to the energy released during the adsorption of the relaxed adsorbate components on the substrate. Higher negative adsorption energy values indicate a more stabilized and stronger interaction between a metal and an inhibitor molecule [Verma *et al.* (2015) (b)]. It can be seen from the results, that the negative values of adsorption energies of nicotinonitriles on Fe (110) surface shows the following order AMN > ATN. This ordering is in good agreement with the observed experimental inhibition efficiency for ATN and AMN.

3.2 Naphthyridines as corrosion inhibitors

Naphthyridines show various biological activities such as antibacterial, antiviral and antiproliferative activities, and also act as an inhibitor of human immunodeficiency virus (HIV) infection [Insuasty *et al*.(2013)], [Deyanov *et al*.(1991)], [Grossi *et al*.(2005)], [Hameed *et al*.(2015)]. They can be chosen as corrosion inhibitors because of their fascinating structural features like heteroatoms, aromatic rings and π-bonds in their molecules. A few of naphthyridines have been tested as corrosion inhibitors. Ansari and Quraishi have reported three naphthyridines namely 2-amino-4-(4-methoxyphenyl)-1,8-naphthyridine-3-carbonitrile (ANC-1), 2-amino-4-(4 methylphenyl)-1,8-naphthyridine-3-carbonitrile (ANC-2) and 2-amino-4-(3-nitrophenyl)-1,8-naphthyridine-3-carbonitrile (ANC-3) exhibited 93.9%, 91.4% and 85.0% inhibition efficiencies respectively at 200 mg/l for N80 steel in 15% hydrochloric acid [Ansari and Quraishi (2015) (a)].

In the current study, three naphthyridines namely, 5-amino-9-hydroxy-2-phenylchromeno[4,3,2-de][1,6]naphthyridine-4-carbonitrile (N-1), 5-amino-9-hydroxy-2-(p-tolyl)chromeno[4,3,2-de][1,6]naphthyridine-4-carbonitrile (N-2), and 5-amino-9-hydroxy-2-(4-methoxyphenyl)chromeno[4,3,2-de][1,6]naphthyridine-4-carbonitrile (N-3) have been selected as corrosion inhibitors. The objective is to investigate the corrosion inhibition effect of the naphthyridines along with the electronic and steric effects of the substituent groups for MS in 1 M hydrochloric acid solution using different techniques such as weight loss, electrochemical impedance spectroscopy (EIS) and potentiodynamic polarization. The Surface analyses were carried out by using scanning electron microscopy (SEM) and atomic force microscopy (AFM). Quantum chemical calculations were also carried out in order to investigate the correlations

between experimental observations and quantum chemically derived reactivity indices. Monte Carlo simulations were performed to model the adsorption of the studied compounds on Fe (110) surface and to predict the adsorption energies, which were later correlated with the experimental results.

3.2.1 Weight loss measurements

3.2.1.1 Effect of inhibitor concentrations

The results obtained from the weight loss measurements, such as corrosion rate and corrosion inhibition efficiency are listed in Table 3.2.1, which shows that on addition of different concentrations of N-1, N-2, and N-3, the inhibition efficiency increases and the corrosion rate decreases. The efficiency-concentration profile is shown in Figure 3.2.1.

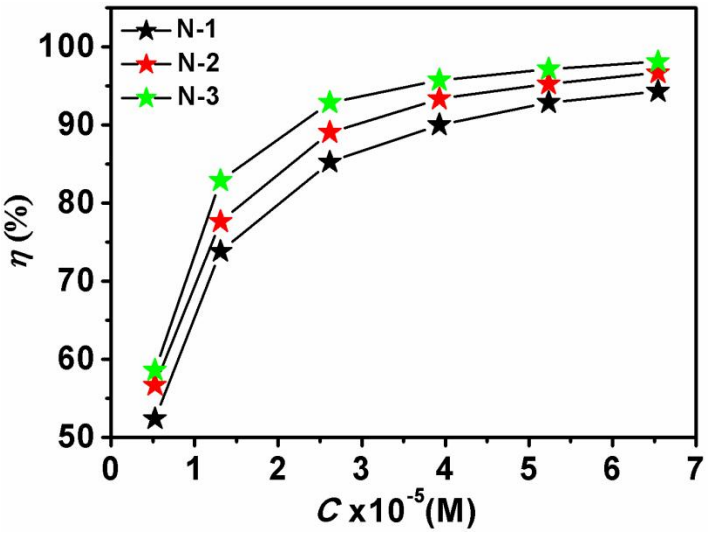

Figure 3.2.1 Effect of different concentrations of Naphthyridines on corrosion inhibition efficiency for MS in 1 M HCl.

The increase in corrosion inhibition efficiency with concentration is attributed to adsorption of more inhibitor molecules that forms protective film on MS surface [Singh *et al.* (2014) (a)], [Yadav *et al.* (2012) (a)]. The difference in inhibition efficiency is

attributed to substituent groups attached to the para position of the phenyl ring of N-1, N-2, and N-3,(-OCH_3, -CH_3, -H). The N-3 and N-2 shows the highest inhibition efficiency due to presence of electron releasing group (-CH_3O and -CH_3) in benzene ring, than N-1which is devoid of any substituent [Verma *et al.* (2015) (a)], [Yadav *et al.* (2013) (b)].

Table 3.2.1 Weight loss measurements for MS in absence and presence of Naphthyridines in 1 M HCl at 308 K.

Inhibitors	Concentrations (M x 10^{-5})	Corrosion rate (mm/y)	Surface coverage (θ)	η%
Blank	0.0	77.9	-	-
N-1	0.52	37.1	0.52	52.38
	1.30	20.4	0.73	73.80
	2.61	11.5	0.85	85.23
	3.92	7.7	0.90	90.00
	5.23	5.5	0.92	92.85
	6.54	4.4	0.94	94.28
N-2	0.52	33.7	0.56	56.66
	1.30	17.4	0.77	77.61
	2.61	8.5	0.89	89.04
	3.92	5.1	0.93	93.33
	5.23	3.7	0.95	95.23
	6.54	2.5	0.96	96.66
N-3	0.52	32.2	0.58	58.57
	1.30	13.3	0.82	82.85
	2.61	5.5	0.92	92.85
	3.92	3.3	0.95	95.71
	5.23	2.2	0.97	97.14
	6.54	1.4	0.98	98.09

3.2.1.2 Effect of Temperature

The effect of temperature (308-338 K) on corrosion inhibition efficiency for MS at optimum concentration is shown in Figure 3.2.2. It is clearly seen from the plot that corrosion inhibition efficiency for all the studied Naphthyridines decreases upon

increase in temperature, that suggesting desorption of adsorbed inhibitor molecules from the MS surface at higher temperatures [Ansari and Quraishi (2014)].

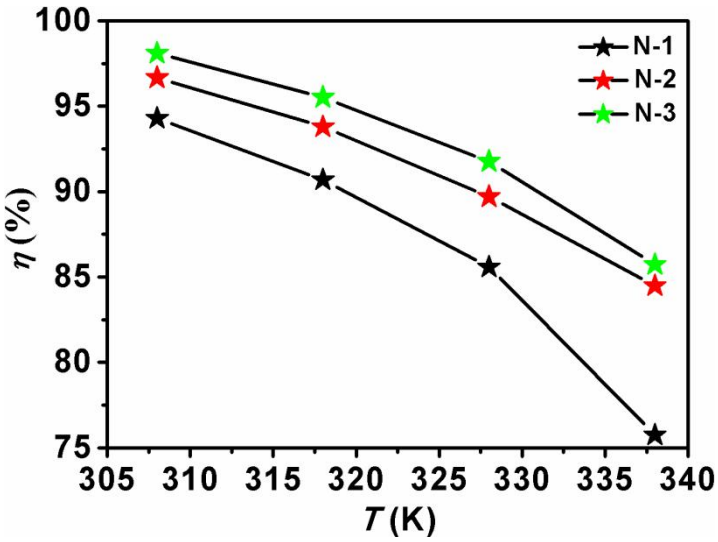

Figure 3.2.2 Effect of temperature (308-338 K) on corrosion inhibition efficiency for MS in presence of Naphthyridines in 1 M HCl.

3.2.1.3 Adsorption isotherm

Adsorption isotherms are used to understand the mode of interactions between inhibitor molecules and metal surface [Sasikumar *et al.* (2015)], [Umoren *et al.* (2014)].

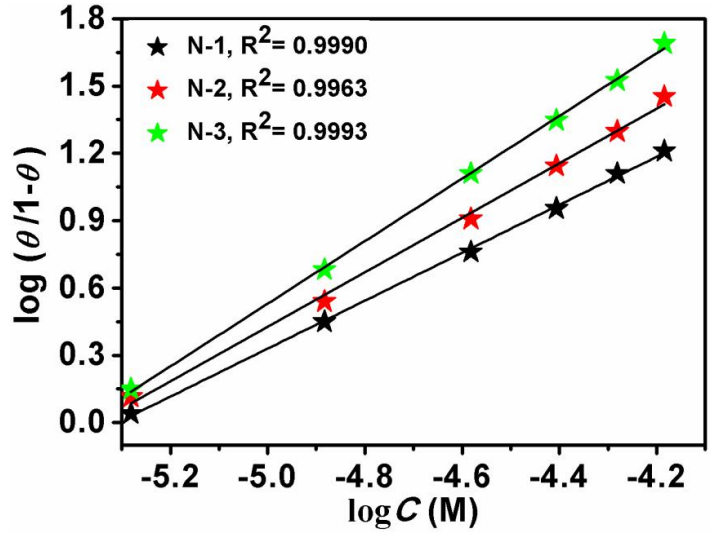

Figure 3.2.3 Langmuir adsorption isotherm plot for MS in presence of Naphthyridines.

The experimental data were subjected into various adsorption isotherms. Langmuir adsorption isotherm (Figure 3.2.3) gave the best fit with R^2 values close to 1 for N-1, N-2, and N-3.

The calculated values of ΔG_{ads} are listed in Table 3.2.2. The ΔG_{ads} values obtained in the present study range from -42 to -43 kJ mol^{-1}, which suggests both physical as well as chemical mode of adsorption but predominantly chemisorption [Solmaz (2014) (a)], [Solmaz(2014) (b)].

Table 3.2.2 ΔG_{ads} at optimum concentration of Naphthyridines for MS in 1 M HCl at 308-338 K.

Inhibitors	Temperature	ΔG_{ads} (kJ mol^{-1})
N-1	308	-42.10
	318	-42.09
	328	-42.07
	338	-41.56
N-2	308	-43.53
	318	-43.24
	328	-43.14
	338	-43.11
N-3	308	-44.93
	318	-44.18
	328	-43.78
	338	-43.40

3.2.2 Electrochemical measurements

3.2.2.1 Electrochemical impedance spectroscopy

The Nyquist loops, equivalent circuit model and Bode-phase angle plots are presented in Figure 3.2.4 (a-c) respectively and the observed electrochemical kinetic parameters are listed in Table 3.2.3. In the studied frequency range the Nyquist loop exhibited semicircle capacitive loop. Figure 3.2.4 (a) shows that obtained Nyquist loops are depressed semicircles with the centers under the real axis. This can be attributed to

the rough surface, frequency dispersion, relaxation and porosity in mass transport effects [Sudheer and Quraishi (2014)], [Yadav *et al.* (2015)].

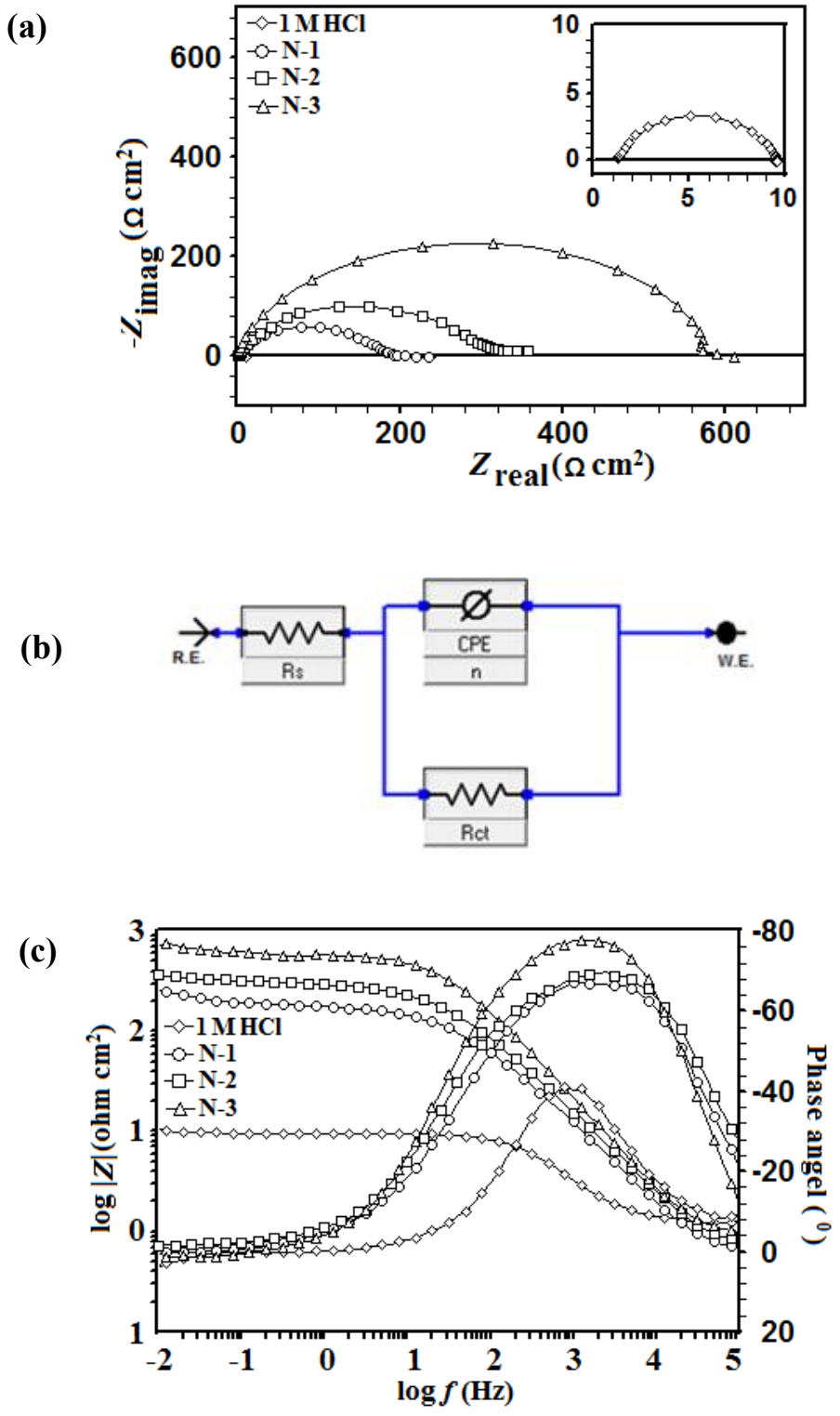

Figure 3.2.4 (a) Nyquist plots (b) Equivalent circuit model and (c) Bode-phase angle plots for MS in 1 M HCl without and with Naphthyridines.

In view of these points, a constant phase element (CPE) must be introduced to the equivalent model for accurate fit, consisting R_s (solution resistance), CPE (constant-phase element), which is parallel to charge transfer resistance (R_{ct}). The results listed in Table 3.2.3 show that the R_{ct} values are higher in presence of naphthyridines than in the blank solution and the maximum of 569.91 Ω cm^2 was obtained for N-3 at 6.54 x 10^{-5} M. The decrease in C_{dl} values in presence of naphthyridines implies that the inhibitors form protective film on the MS surface [Ansari *et al.* (2015)].

Table 3.2.3 Electrochemical Impedance Parameters for MS in absence and presence of Naphthyridines in 1 M HCl.

Inhibitors	Concentrations (M x 10^{-5})	R_{ct} (Ω cm^2)	C_{dl}	η%	$-S$	$-\alpha°$
Blank	0.0	9.0	106	-	0.53	40.40
N-1	6.54	187.31	27	95.19	0.75	66.94
N-2	6.54	319.89	24	97.18	0.77	68.48
N-3	6.54	569.91	11	98.42	0.90	77.84

The ideal capacitive behaviour for Bode and phase angle would result, if the slope value attains -1 and phase angle value attains -90° at the intermediate frequencies. In the presence of N-1, N-2, and N-3 as shown in Figure 3.2.4 (c) the respective values of the slope and phase angle range from 0.75 to 0.90, and 67° to 77° as compared to those of the blank solution i.e. 0.53 and 40.40 respectively, suggesting non-ideal behaviour of the capacitor [Dandia *et al*. (2013)].

3.2.2.2 Potentiodynamic polarization measurements

The comparative polarization curves for MS in the absence and presence of N-1, N-2, and N-3 are shown in Figure 3.2.5 and the corresponding parameters such as corrosion potential, E_{corr} and corrosion current density, i_{corr} are listed in Table 3.2.4.

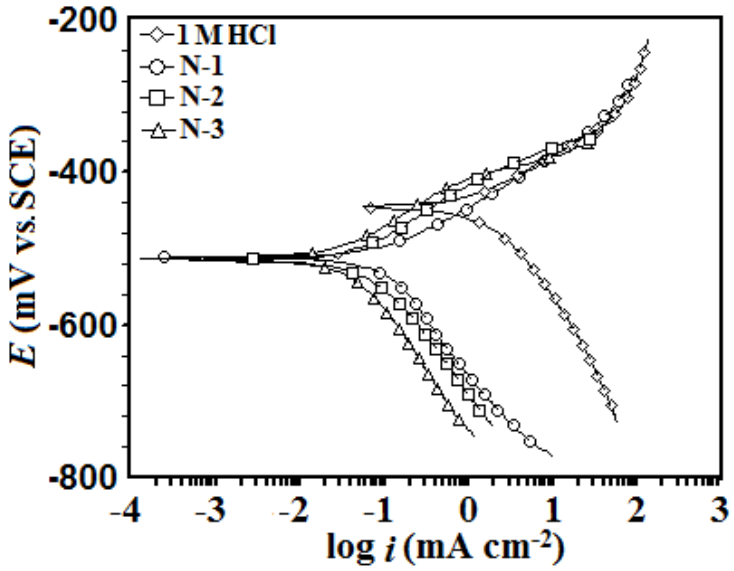

Figure 3.2.5 Polarization curves for MS in 1 M HCl without and with Naphthyridines at 6.54 x 10^{-5} M.

The presence of naphthyridines shifted corrosion potential for MS between 67-70 mV cathodically, which is less than 85 mV [Kosari *et al.* (2014)], [Yadav and Quraishi (2012) (a)]. This indicates that N-1, N-2, and N-3 act as mixed-type inhibitor with predominant cathodic inhibition effect. The reduction in i_{corr} values in the presence of the naphthyridines confirms corrosion inhibition for MS due to adsorption of inhibitor molecules on MS surface [Yadav and Quraishi (2012) (b)].

Table 3.2.4 Polarization parameters for MS in absence and presence of Naphthyridines in 1 M HCl.

Inhibitors	Concentrations (M x 10^{-5})	i_{corr} (µAcm-^{2})	E_{corr} (mV/SCE)	η%
Blank	0.0	1390	-445	-
N-1	6.54	42	-512	96.97
N-2	6.54	22	-515	98.20
N-3	6.54	13	-513	99.06

3.2.3 Surface characterization

The SEM micrographs for MS in absence and presence of N-1, N-2, and N-3 are shown in Figure 3.2.6 (a-d). The SEM image without inhibitor is highly corroded (Figure 3.2.6 (a)), resulting in a rough and heterogeneous surface of MS in 1 M HCl. But in the presence of the studied naphthyridines the MS surface is smoother, which confirms their inhibition action as shown in Figures 3.2.6 (b-d) [Yadav *et al*. (2013) (a)].

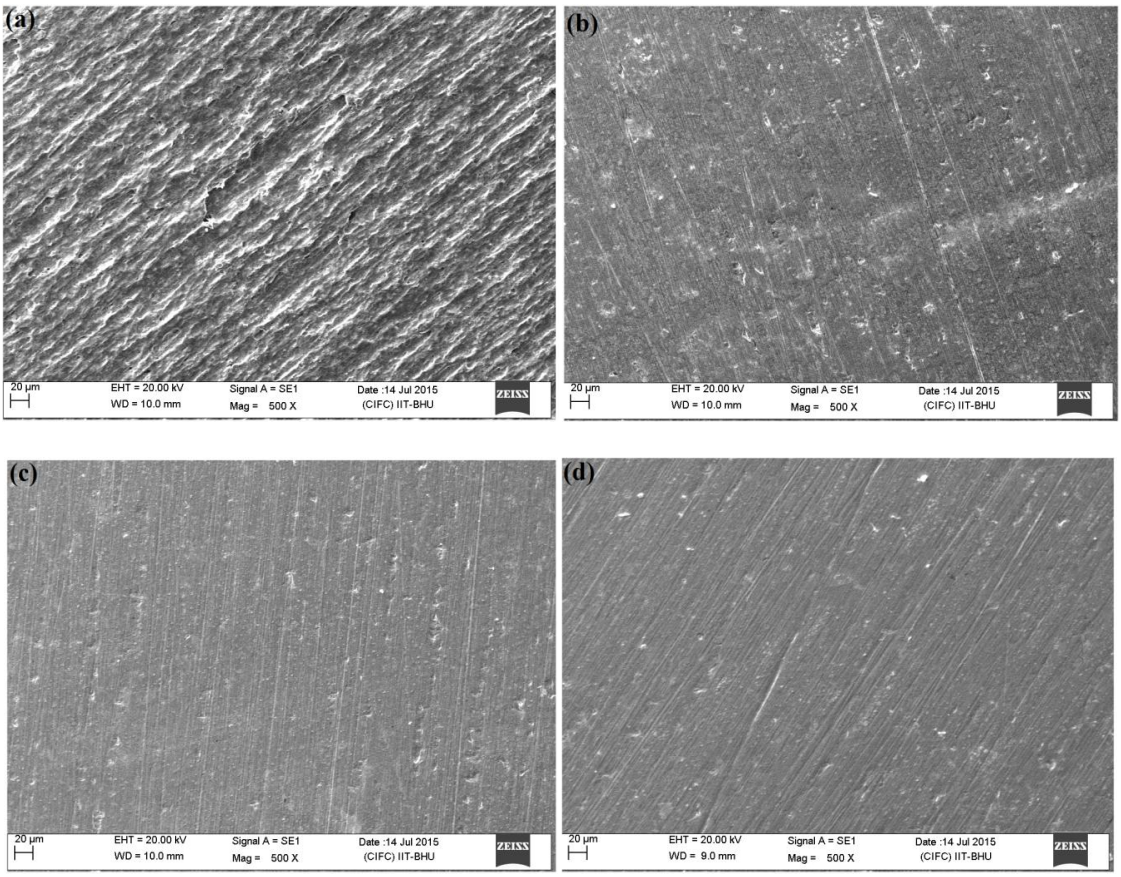

Figure 3.2.6 (a-d) SEM micrographs for MS in (a) 1 M HCl and in presence of inhibitors (b) N-1, (c) N-2, and (d) N-3 at 6.54 x 10^{-5} M.

AFM is another useful method for the surface analysis [Mourya *et al.* (2014)]. In the absence of naphthyridines the surface displayed an extremely rough topography due to unhindered acid attack (Figure 3.2.7 (a)) while in presence of N-1, N-2, and N-3, the MS shows smoother surface (Figure 3.2.7 (b-d)). Both the surface studies supported the corrosion inhibition for MS in presence of inhibitors.

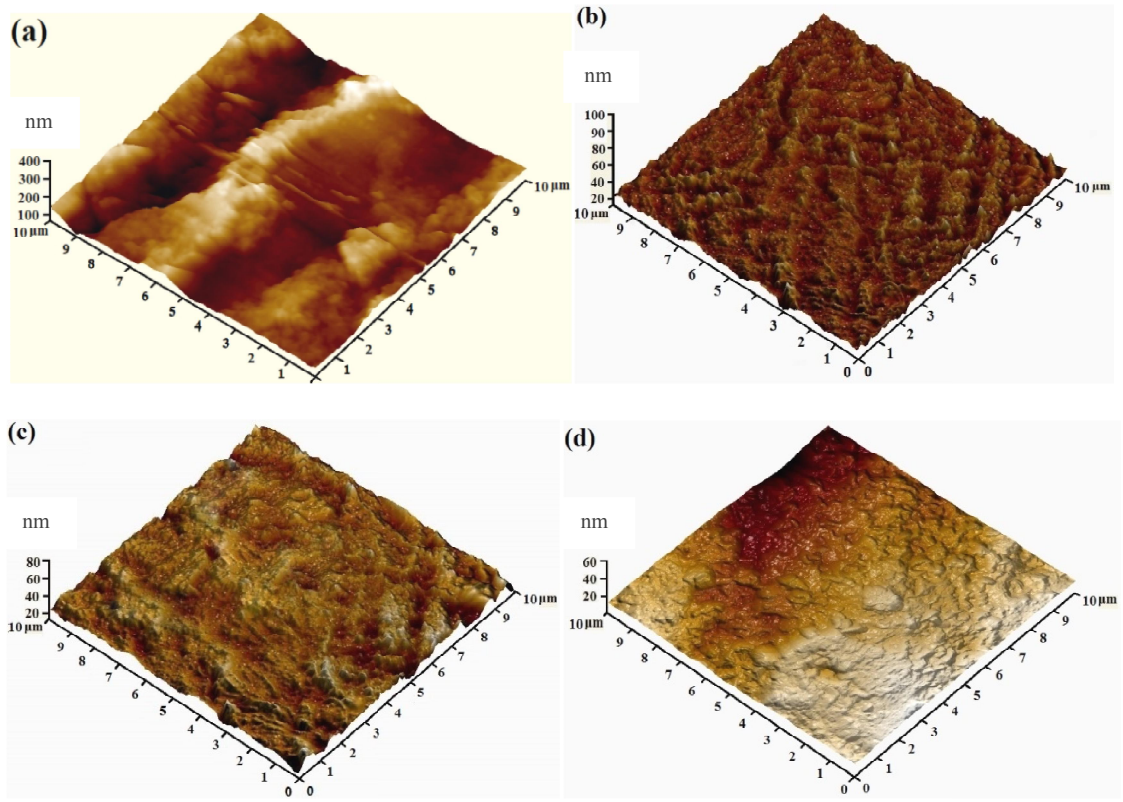

Figure 3.2.7 (a-d) AFM micrographs for MS (a) in 1 M HCl and in presence of inhibitors (b) N-1, (c) N-2, and (d) N-3 at 6.54 x 10^{-5} M.

3.2.4 Quantum chemical calculations

The gas phase optimized molecular structures and the respective HOMO and LUMO electron density surfaces of the studied compounds are shown in Figure 3.2.8. The optimized structures revealed that the molecules of the studied compounds adopt near planar geometries in which the 2-aryl substituents are only slightly twisted.

The near planar geometries of these compounds might contribute to their high inhibition efficiencies because high degree of planarity has been reported to favour optimum adsorption of inhibitor molecules on metal surface leading to enhanced inhibition efficiency [Ebenso *et al.* (2012)], [Arslan *et al.* (2009)], [Bentiss and Lagrenee (2011)].

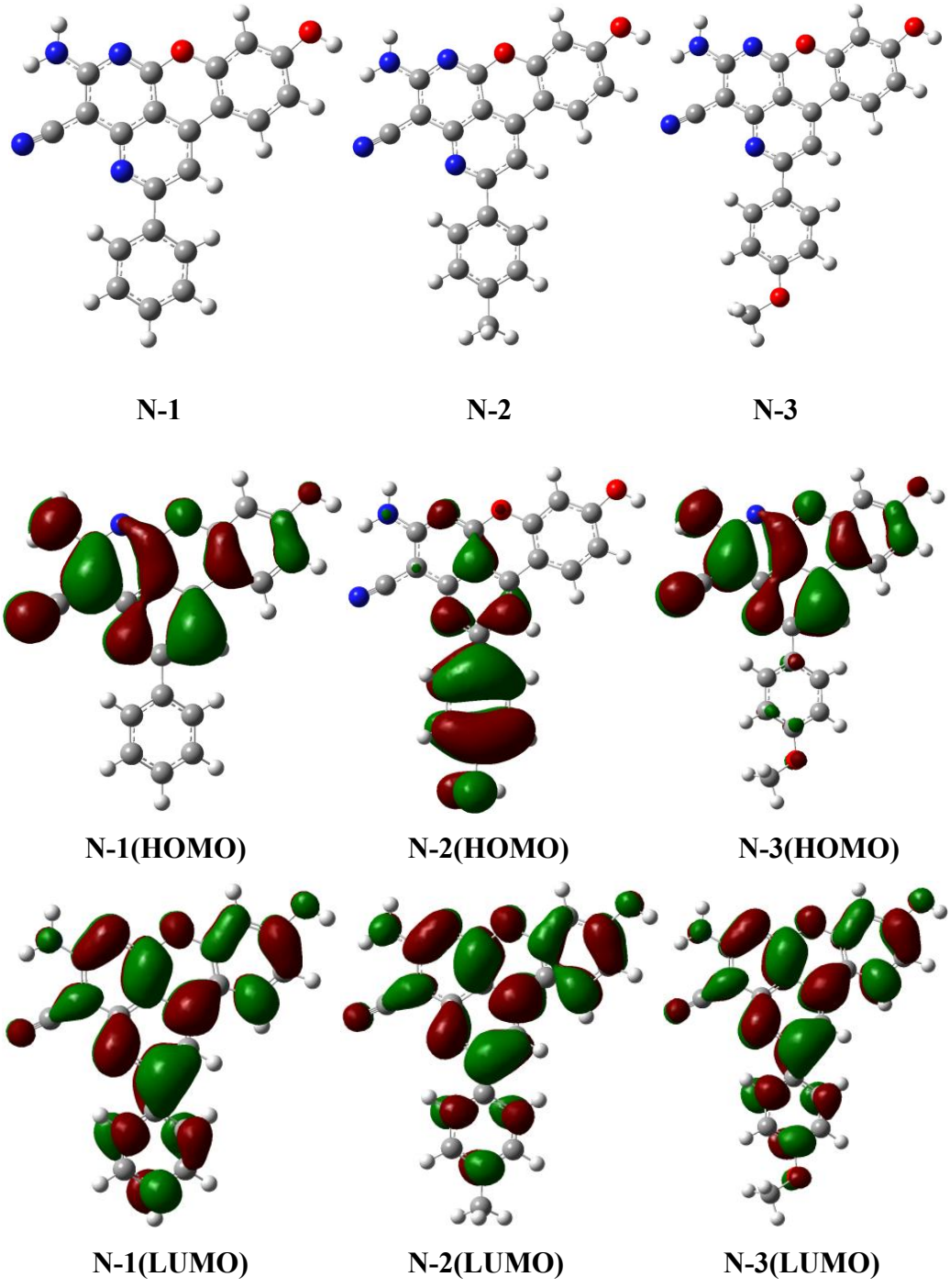

Figure 3.2.8 The gas phase optimized molecular structures, the HOMO, and the LUMO electron density distribution surfaces of N-1, N-2, and N-3.

The HOMO electron density surface provides information about the sites of the molecule that are most likely to donate electrons to the appropriate orbital of an acceptor species, while the LUMO electron density surface suggests the sites of the molecule that possess higher chances of accepting electrons from a donor species. The FMO electron density distribution of the studied compounds exhibit similar features of the LUMO but clearly different HOMO surfaces. For this reason, the variation in the inhibition efficiencies of the studied molecules might not be describable based on the LUMOs. Both the HOMOs and the LUMOs of the studied molecules comprise the π-type orbital, which suggests that the molecules can favourably interact with the vacant/filled d- or p- orbitals of the metal atom. The HOMO of N-1 is widely distributed over all the rings in the molecule except the 2-phenyl substituent, which does not contribute to the HOMO. The HOMO of N-2 on the other hand is well delocalized over the p-tolyl substituent and slightly extended to a few carbon atoms in the other rings. The HOMO of N-3 just like N-1 is also delocalized over the entire rings in the molecule but unlike N-2, the atoms of the 4-methoxyphenyl group in N-3 also makes little contributions to the HOMO. The effects of the methyl and methoxy substituents present in N-2 and N-3 respectively are very apparent in the HOMO electron density distributions.

The values of some quantum chemical parameters obtained for the studied compounds both in the gas and water phases are listed in Table 3.2.5. The values of the E_{HOMO} obtained for the studied compounds in the gas and water phases are in the order: N-3 > N-2 > N-1, which agrees with the order of the experimental inhibition efficiencies. The results of the E_{LUMO} in Table 3.2.5 do not agree with the trend of the observed inhibition efficiencies. This observation is in line with the similar LUMO surfaces of the

molecules, which suggests that the E_{LUMO} may not be a good descriptor for the relative inhibition efficiency of the studied molecules.

Table 3.2.5 Quantum chemical parameters derived from the B3LYP/6-31+G (d,p) method of the studied compounds.

Parameters→ Compounds↓	E_{HOMO} **(eV)**	E_{LUMO} **(eV)**	ΔE **(eV)**	χ **(eV)**	ΔN
In Vacuo					
N-1	-6.039	-2.397	3.642	4.218	0.764
N-2	-5.996	-2.340	3.656	4.168	0.775
N-3	-5.961	-2.287	3.673	4.124	0.783
In Water					
N-1	-6.134	-2.439	3.695	4.286	0.734
N-2	-6.116	-2.408	3.708	4.262	0.738
N-3	-6.086	-2.378	3.707	4.232	0.747

The energy gap, ΔE is another index of reactivity of molecules for which molecules with lower ΔE are usually more reactive and possess higher inhibition efficiency. The trend of the ΔE values obtained for the studied compounds is not in agreement with the experimental inhibition efficiencies. This is not unexpected because the E_{LUMO} values do not correlate with the experimental results and the ΔE is derived from the E_{HOMO} and E_{LUMO}. The global electronegativity, χ is another reactivity index that predicts the extent to which a molecule retains its electrons. The higher the χ the lower the chance of electron donation by the molecule and vice versa. The trends of the values of χ obtained for the studied compounds in the gas and water phases as shown in Table 3.2.5 are N-3 < N-2 < N-1, which suggests that N-3 has the highest possibility of donating electrons to an electrophilic centre such as the iron surface that is populated by positive charges. The trend of χ is in agreement with the experimental inhibition efficiencies. The values of ΔN, i.e. fraction of the electrons moved via the inhibitor molecule to the metal [Tehrani and Niazi (2015)] as reported in Table 3.2.5 also corroborate the trend of the

experimental inhibition efficiencies. The ΔN values suggest that the order of fraction of electrons moved by the inhibitor molecule to iron is as: N-3 > N-2 > N-1 both in the gas and water phases. The quantum chemical parameters (E_{HOMO}, χ, and ΔN) that showed good agreement with the experimental results are those that suggest high inhibition efficiency for an inhibitor with a good electron-donating ability. This suggests that the mode of adsorption of the studied molecules on the MS surface is predominantly via electron donation from the high electron density sites of the molecules to the iron. The practicality of this assumption also rests on the fact that the surface of MS in acidic medium is reportedly populated by positive charges [Lebrini *et al.* (2005)], [Ebenso *et al.* (2010)] such that the interaction of electron donating inhibitor molecules with the positively charged MS surface is a favourable process.

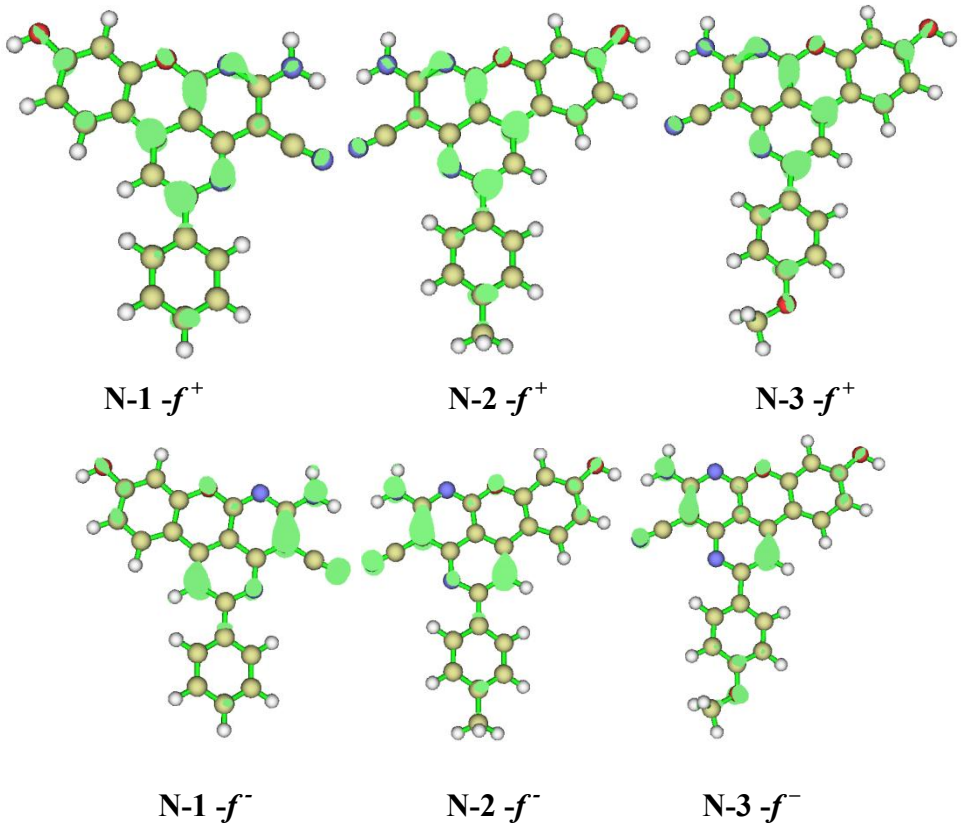

Figure 3.2.9 The gas phase Fukui indices for the electrophilic (f_k^+) and nucleophilic (f_k^-) sites in N-1, N-2, and N-3 (isosurface value = 0.003).

The Fukui indices, f_k^+ and f_k^- were calculated to predict the most probable atomic sites for electrophilic and nucleophilic activities respectively. The electron density surfaces of the f_k^+ and f_k^- are shown in Figures 3.2.9. The region of the molecules with higher values of f_k^+ are more susceptible to the attack by electron rich species, while the sites of the molecules with higher values of f_k^- are more disposed to interactions with electron deficient species. As shown in Figure 3.2.9, the sites for both the f^+ and f^- are essentially found on the chromeno-naphthyridine rings, while the atoms of the 2-aryl substituent in each case do not exhibit significant reactivity. The N atoms of the Naphthyridine and the C atom directly connected to the aryl substituents show high density of f^+ and therefore represent the most probable sites with which the studied compounds can interact with a negatively charged metal surface. The N atoms of the amino and carbonitrile groups as well as the carbon atoms directly adjacent to them exhibit high density of f^-, which suggests that they are among the most probable sites from which electrons can be donated to positively charged metal surface.

3.2.5 Monte Carlo simulation

The Monte Carlo simulations help to predict the interaction between the inhibitor molecules and metal surface. Figure 3.2.10, shows a typical plot of energy distribution (total energy, average total energy, vander waals energy, electrostatic energy and intermolecular energy) for N-3 with Fe (110) surface during the energy optimization process. The most stable low energy adsorption configurations of (a) N-1, (b) N-2 and (c) N-3 on Fe (110) surface were simulated by MC simulation and the configurations are shown in Figure 3.2.11. The resulting energy parameters including the total energy, adsorption energy, rigid adsorption and deformation energies are listed in Table 3.2.6.

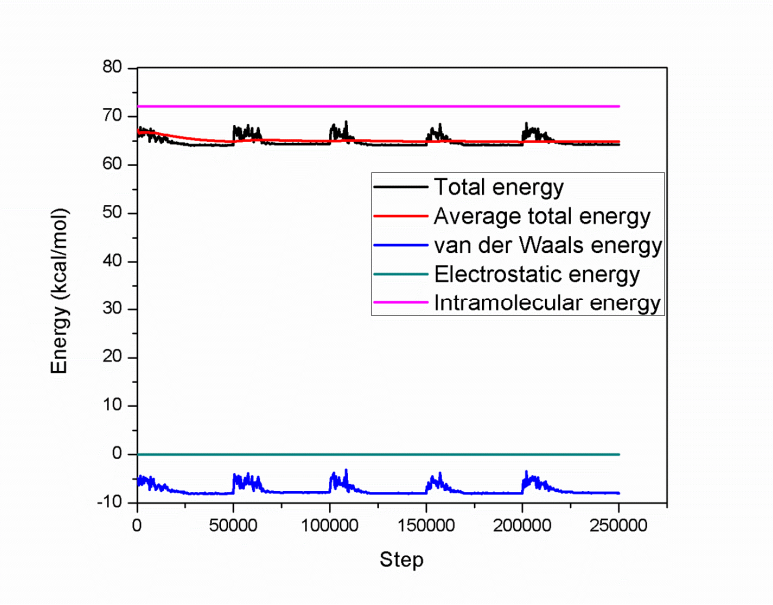

Figure 3.2.10 A typical energy profile for the adsorption of N-3 on Fe (110) surface obtained using the Monte Carlo simulations.

The adsorption energy is attributed to the energy released during the relaxed adsorbate components adsorbed on the substrate. The adsorption energy is the combination of rigid adsorption and deformation energies of the adsorbate component. Higher negative adsorption energy values indicate a more stabilized and stronger interaction between a metal and an inhibitor molecule [Ramaganthan *et al.* (2015)].

Table 3.2.6 Outputs and descriptors calculated by the Monte Carlo simulation for the most stable adsorption configurations of N-1, N-2 and N-3 on Fe (110) surface (all units in kcal/mol).

Systems	Total Energy	Adsorption energy	Rigid adsorption energy	Deformation energy	dE_{ad}/dN_i Inhibitors
Fe(110)/N-1	56.478	-8.024	-8.152	0.128	-8.024
Fe(110)/N-2	57.212	-8.376	-8.503	0.127	-8.376
Fe(110)/N-3	63.681	-8.469	-8.764	0.294	-8.469

It can be seen from the results in Table 3.2.6, that the negative values of adsorption energies of naphthyridines on Fe (110) surface increase in following order N-3>N-2>N-1 which is in good agreement with the experimental inhibition efficiency values.

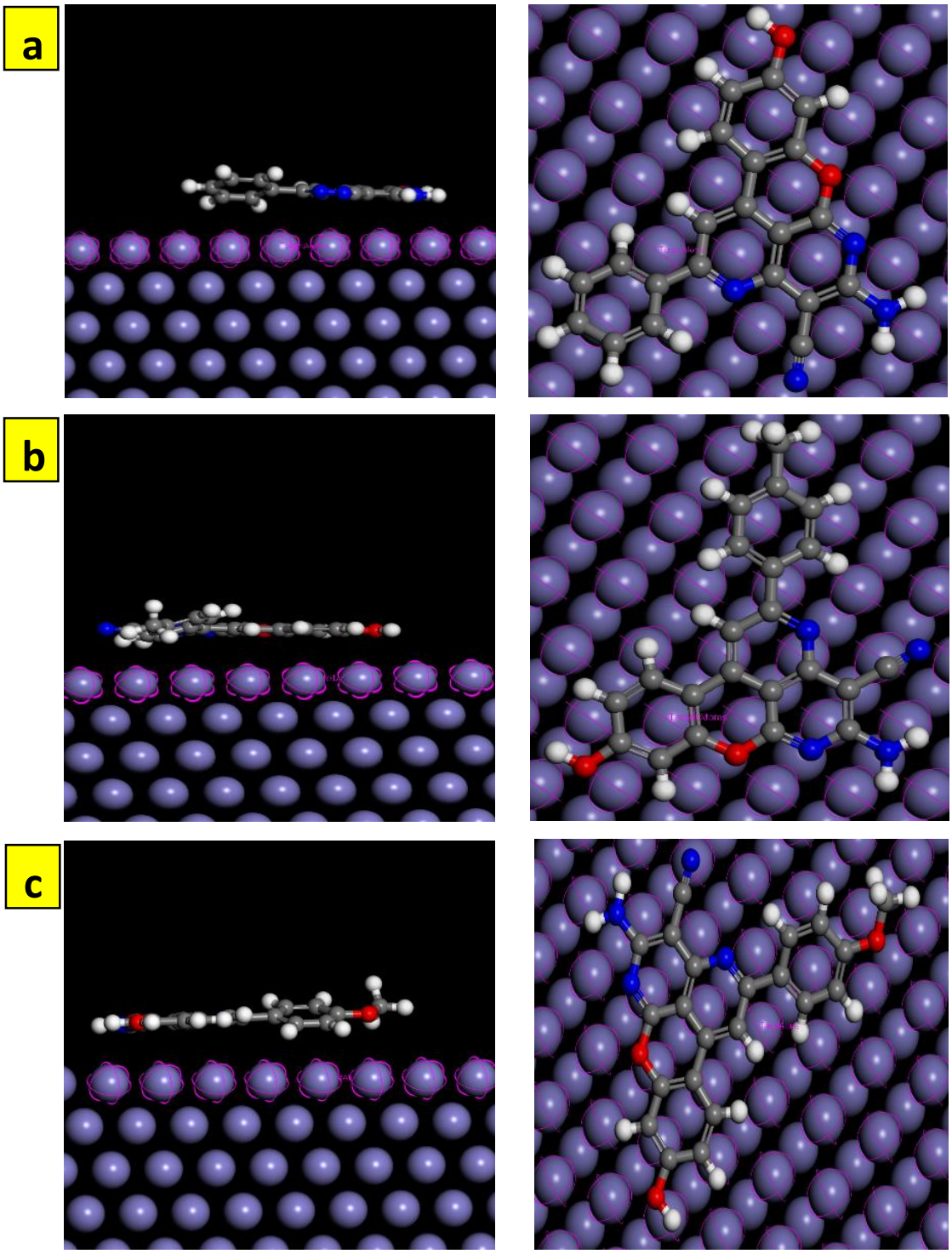

Figure 3.2.11 Side and top views of the most stable low energy configuration for the adsorption of (a) N-1, (b) N-2 and (c) N-3 on Fe (110) surface obtained by Monte Carlo Simulations.

3.3 Quinolines as corrosion inhibitors

Quinolines constitute a class of heterocyclic aromatic compounds having double-ring structure in which the benzene ring is fused with pyridine by two adjacent carbon atoms. Quinoline ring is found in a large number of natural products and can be used commercially in pharmaceuticals, fragrances, and dyes. Quinoline compounds are widely used as "parental" compounds to synthesize molecules with medicinal benefits. Drugs containing quinoline ring such as quinine, chloroquine, mefloquine, and amodiaquine are used for the treatment of malaria [Keri and Patil (2014)], [Afzal *et al.* (2014)]. In view of non-toxic nature and biological activities quinolines can be tested as corrosion inhibitors. There are only a few reports on the use of quinoline derivatives as corrosion inhibitors [Ramesh and Adhikari (2009)], [Saliyan and Adhikari (2008)].

In the present investigation, four quinoline derivatives namely 2-amino-7-hydroxy-4-phenyl-1,4-dihydroquinoline-3-carbonitrile (Q-1), 2-amino-7-hydroxy-4-(p-tolyl)-1,4 dihydroquinoline-3-carbonitrile (Q-2), 2-amino-7-hydroxy-4-(4-methoxyphenyl)-1,4 dihydroquinoline-3 carbonitrile (Q-3), 2-amino-4-(4-(dimethylamino)phenyl)-7-hydroxy-1,4-dihydroquinoline-3-carbonitrile (Q-4) have been chosen as corrosion inhibitors. The aim of the work is to investigate their inhibiting action on the corrosion of mild steel in 1 M HCl using weight loss, electrochemical techniques (impedance spectroscopy (EIS) and potentiodynamic polarization). SEM, AFM, and XPS techniques were used for surface analysis of mild steel specimens.

3.3.1 Weight loss measurements

3.3.1.1 Effect of inhibitor concentration

The results obtained from weight loss study are given in Table 3.3.1 and the effect of inhibitor concentrations on corrosion inhibition efficiency is shown in Figure 3.3.1.

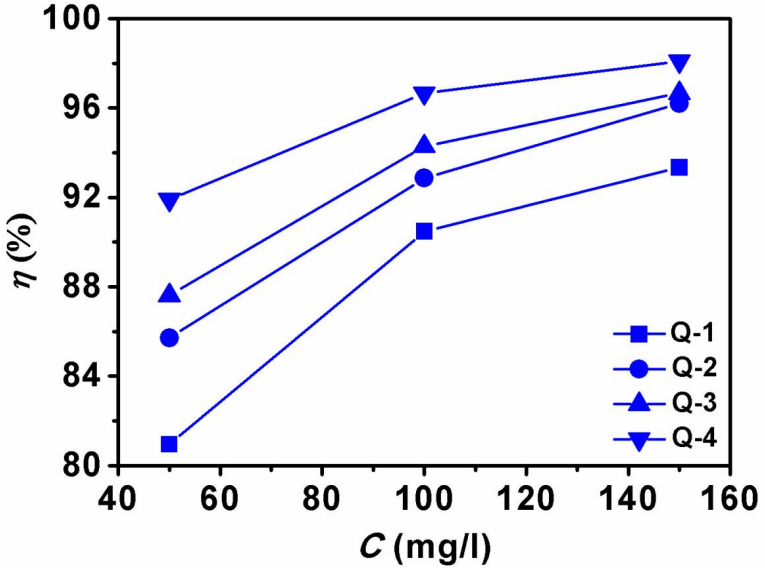

Figure 3.3.1 Effect of different concentrations of Quinolines on inhibition efficiency for MS in 1 M HCl.

It can be seen from the results that on increasing the concentration of inhibitors from 50 to 150 mg L^{-1}, the inhibition efficiency increases from 80.95 to 98.09%. The quinolines show the following order of inhibition Q-4>Q-3>Q-2>Q-1.

Corrosion inhibition performance of a compound depends upon its ability to get adsorbed on metal surfaces. In our investigation, we have taken quinoline derivatives containing π electrons and heteroatoms (N, O) by which they can easily get adsorbed onto the metal surface and form a protective film thereby preventing the corrosion [Singh *et al*. (2013)], [Singh *et al*. (2014) (b)].

Table 3.3.1 Weight loss measurements for MS in absence and presence of Quinoline derivatives in 1 M HCl at 308 K.

Inhibitors	Concentrations (mg L^{-1})	Corrosion rate (mm/y)	Surface coverage (θ)	η%
Blank	0.0	77.9	-	-
Q-1	50	14.8	0.80	80.95
	100	7.4	0.90	90.47
	150	5.1	0.93	93.33
Q -2	50	11.1	0.85	85.71
	100	5.5	0.92	92.85
	150	2.9	0.96	96.19
Q -3	50	9.6	0.87	87.61
	100	4.4	0.94	94.28
	150	2.5	0.96	96.66
Q-4	50	6.3	0.91	91.90
	100	2.5	0.96	96.66
	150	1.4	0.98	98.09

3.3.1.2 Effect of Temperature

Figure 3.3.2 shows the effect of temperature on corrosion inhibition efficiency. The increase in temperature accelerates corrosion reaction and hence shows a decrease in the resultant inhibition efficiency. Increase in temperature causes desorption of inhibitor molecules from the metal surface [Sudheer and Quraishi (2014)].

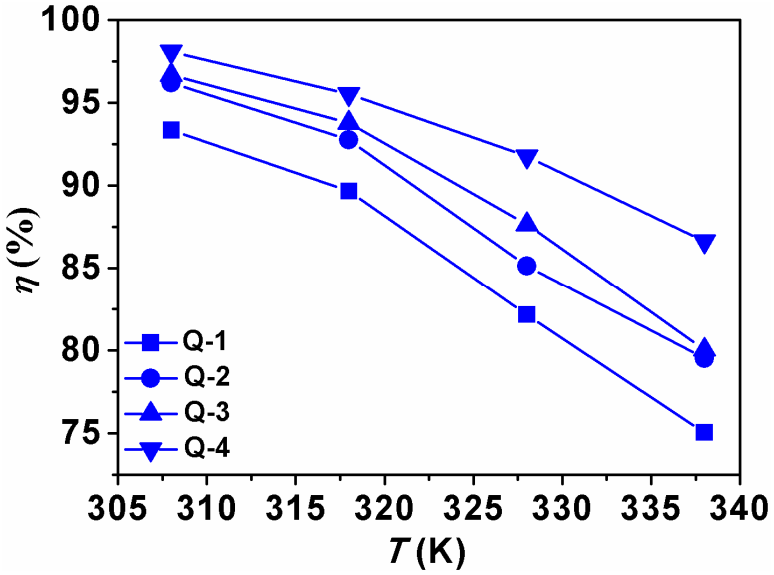

Figure 3.3.2 Effect of temperature (308-338 K) on inhibition efficiency for MS in presence of Quinoline derivatives in 1 M HCl.

The activation energy for MS corrosion in the absence and presence of quinoline derivatives was determined by using Arrhenius equation. A plot between log C_r vs. 1000/T for MS in the absence and presence of inhibitor is presented in Figure 3.3.3 and the corresponding activation parameters are listed in Table 3.3.2. The activation energy is higher for MS in inhibited solution than uninhibited solution due to the creation of an energy barrier which slows down corrosion reaction [Ansari *et al.* (2014)].

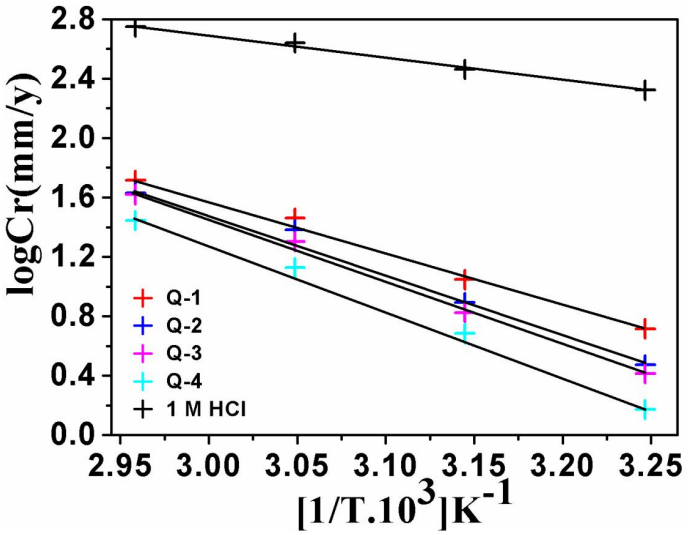

Figure 3.3.3 Arrhenius plots of log C_r vs. 1000/T for MS in the absence and presence of Quinoline derivatives at 150 mg L^{-1} in 1 M HCl.

Table 3.3.2 Activation energy for MS corrosion in absence and presence of Quinoline derivatives in 1 M HCl at 150 mg $L^{-1.}$

Inhibitors	*E*a ($kJmol^{-1}$)
Blank	29.10
Q-1	68.11
Q-2	79.17
Q-3	81.58
Q-4	85.13

3.3.1.3 Adsorption isotherm

The data obtained from the experimental results were fitted to several adsorption isotherms in order to find basic information regarding the interaction of inhibitor molecules and the metal surface. Langmuir isotherm was found to provide the best fitted isotherm with R^2 value close to one (Figure 3.3.4).

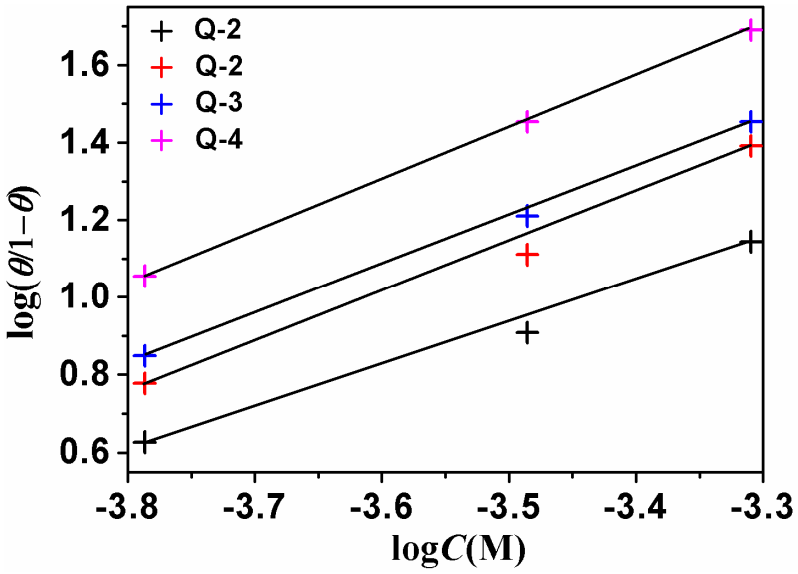

Figure 3.3.4 Langmuir adsorption isotherms for MS in presence of Quinoline derivatives.

The negative values of ΔG_{ads} suggest spontaneous adsorption and stability of the adsorbed layer on MS surface. Also, the ΔG_{ads} values in the range of -20 kJ mol^{-1} indicate electrostatic interaction i.e. (physisorption). On the other hand, a ΔG_{ads} value near or greater than -40 kJ mol^{-1} shows chemisorption [Ramya *et al.* (2014)], [Shaban *et al.* (2015)]. The data listed in Table 3.3.3 show that the ΔG_{ads} values range from -39.7 to -35.8 kJ mol^{-1} suggesting both physical and chemical modes of adsorption but chemical mode is predominant.

Table 3.3.3 ΔG_{ads} for MS in presence of Quinoline derivatives from temperature range 308-338 K at optimum concentration (150 mg L^{-1}).

Inhibitors	Temperature (K)	ΔG_{ads} (kJ mol^{-1})
Q-1	308	-36.43
	318	-36.30
	328	-35.88
	338	-35.80
Q-2	308	-37.94
	318	-37.23
	328	-36.47
	338	-36.43
Q-3	308	-37.94
	318	-37.61
	328	-36.93
	338	-36.60
Q-4	308	-39.77
	318	-38.05
	328	-37.30
	338	-37.81

3.3.2 Electrochemical measurements

3.3.2.1 Electrochemical impedance spectroscopy

Figure 3.3.5 (a) shows the impedance responses of MS in the absence and presence of quinoline derivatives. The impedance parameters calculated from these plots are given in Table 3.3.4.

The Nyquist plots exhibit one capacitive loop in the absence and presence of inhibitors suggesting that corrosion of MS was charge transfer controlled [Ansari and Quraishi (2015) (a)]. The diameter of the capacitive loops increases with increasing concentrations of inhibitors, which suggests that all the four compounds act as effective corrosion inhibitors for MS and showed the following order of inhibition Q-4>Q-3>Q-2>Q-1. The impedance results were analyzed by using the equivalent circuit model shown in Figure 3.3.5 (b).

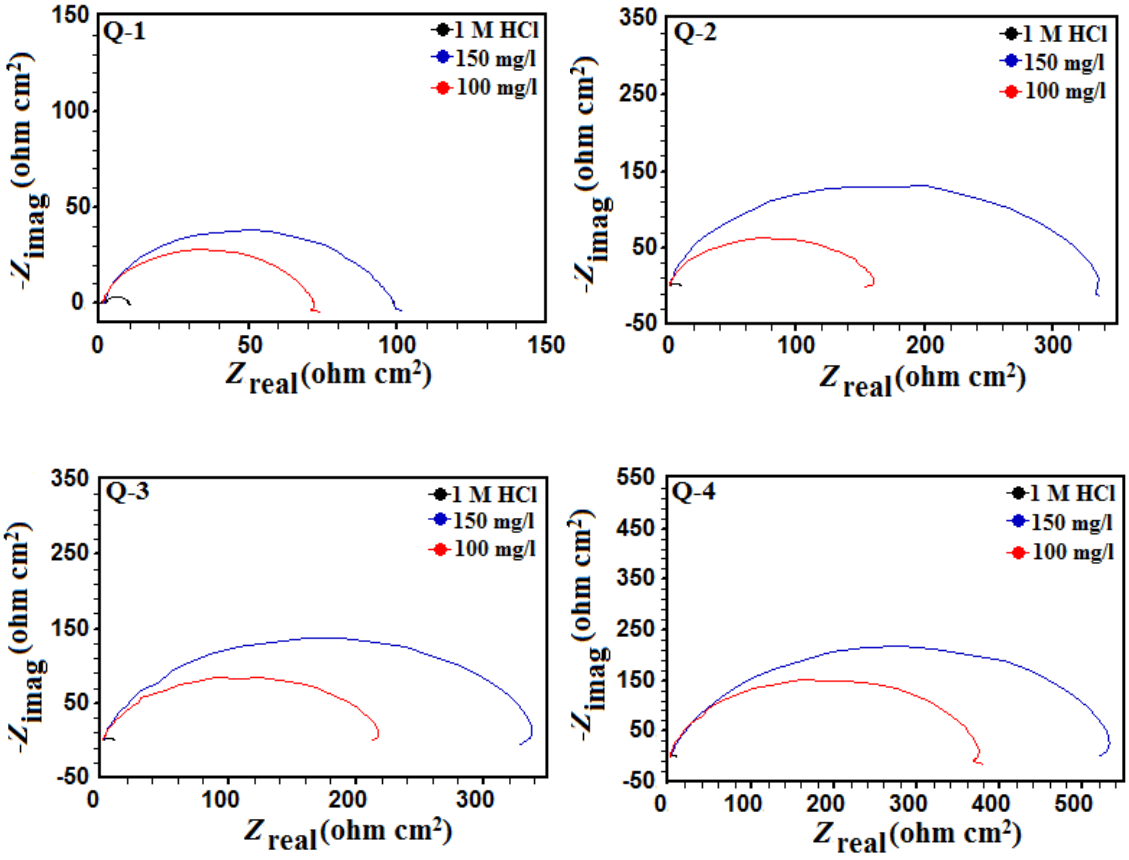

Figure 3.3.5 (a) Nyquist plots for MS without and with Quinoline derivatives in 1 M HCl.

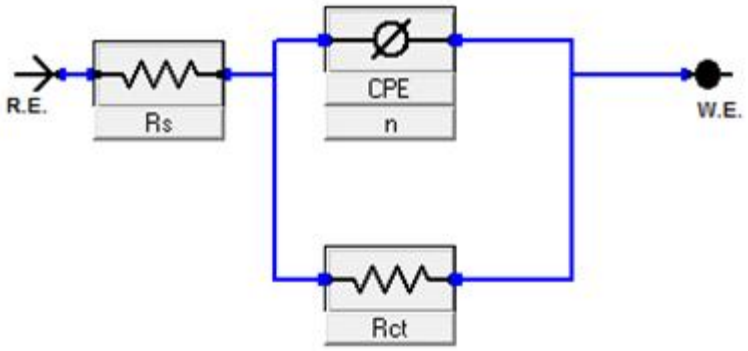

Figure 3.3.5 (b) Equivalent circuit model used to analyze the impedance data.

Table 3.3.4 Electrochemical Impedance Parameters for MS in absence and presence of Quinoline derivatives in 1 M HCl.

Inhibitors	Concentrations (mg L^{-1})	R_{ct} (Ω cm^2)	C_{dl}	η%	$-S$	$-\alpha°$
Blank	0.0	9.0	106	-	0.53	40.40
Q-1	100	69.9	39	87.13	0.82	68.00
	150	97.3	36	90.75	0.83	68.16
Q-2	100	158.6	37	94.32	0.82	70.55
	150	334.9	33	97.31	0.85	74.59
Q-3	100	217.3	35	95.85	0.82	71.02
	150	337.7	33	97.33	0.83	71.54
Q-4	100	373.0	34	97.58	0.80	69.84
	150	546.3	32	98.35	0.88	75.28

The charge-transfer resistances (R_{ct}) were calculated by the difference in impedance at the lower and higher frequencies. The highest R_{ct} is 546.3 Ω cm^2 obtained for Q-4 at 150 mg L^{-1} with 98.35% inhibition efficiency. From the outcome, it can be observed that upon increasing the concentration of inhibitors, the values of R_{ct} increase while a decrease in double layer capacitance C_{dl} is observed. The increase in R_{ct} is attributed to the formation of a protective layer on MS surface [Dasami *et al.* (2015)], [Sangeetha *et al.* (2015)]. In the same manner, a decrease in C_{dl} is attributed to a decrease in dielectric constant and an increase in the thickness of the electrical double layer, suggesting that the inhibitor molecules are adsorbed at the metal/solution interface [Yadav *et al*. (2013) (a)].

The Bode phase angle plots shown in Figure 3.3.5 (c) were recorded for MS in the absence and presence of inhibitors to explain the various phenomena taking place at the metal/solution interface. In our investigation, the Bode slope and phase angle values in the presence of inhibitors range from 0.82 to 0.88 and 68° to 75° and in blank solution 0.53 and 40° as listed in Table 3.3.4. An ideal capacitor behaviour would result

if a slope value attains –1 and phase angle values attain -90° [Solmaz (2014) (a)]. The higher slopes and phase angle values in the presence of inhibitors as compared to blank solution suggesting the formation of a protective film on the MS surface [Yadav and Quraishi (2012) (b)].

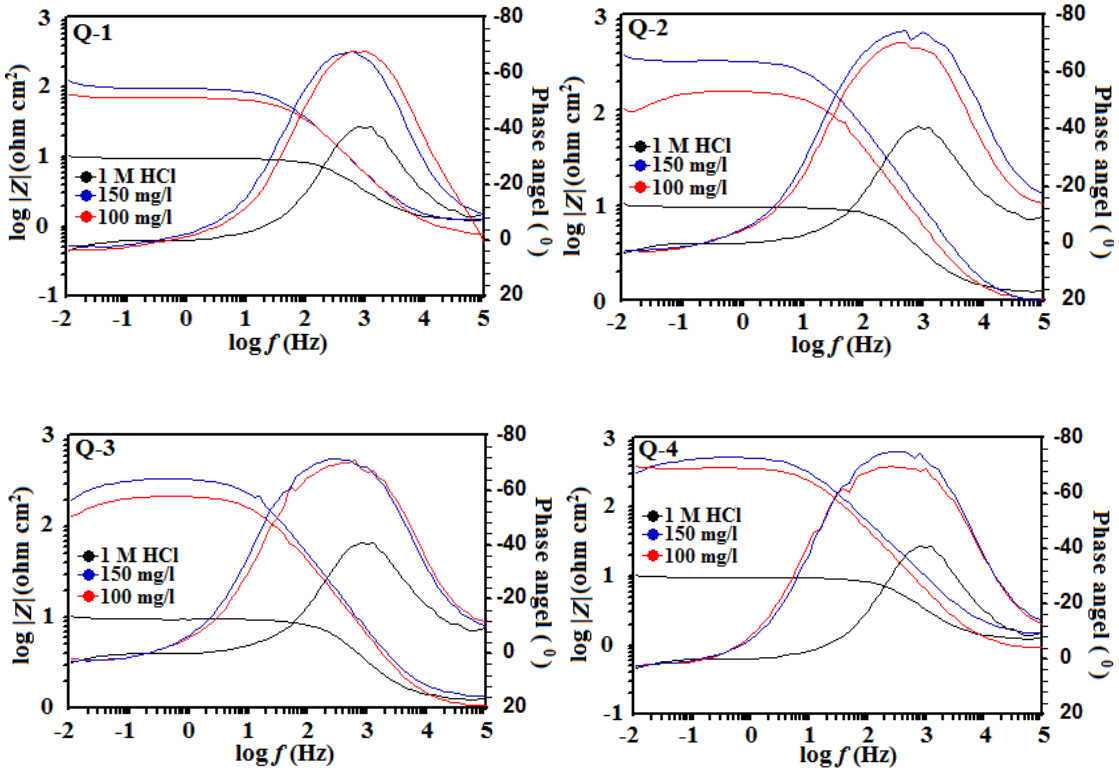

Figure 3.3.5 (c) Bode (log *f* vs log |*Z*|) and phase angle (log *f* vs α) plots of impendance spectra for MS in 1 M HCl containing Quinoline derivatives.

3.3.2.2 Potentiodynamic polarization measurements

The polarization curves for MS in the absence and presence of inhibitors with different concentrations are shown in Figure 3.3.6. The values obtained from polarization curves such as corrosion current densities, i_{corr} and corrosion potential, E_{corr} are listed in Table 3.3.5.

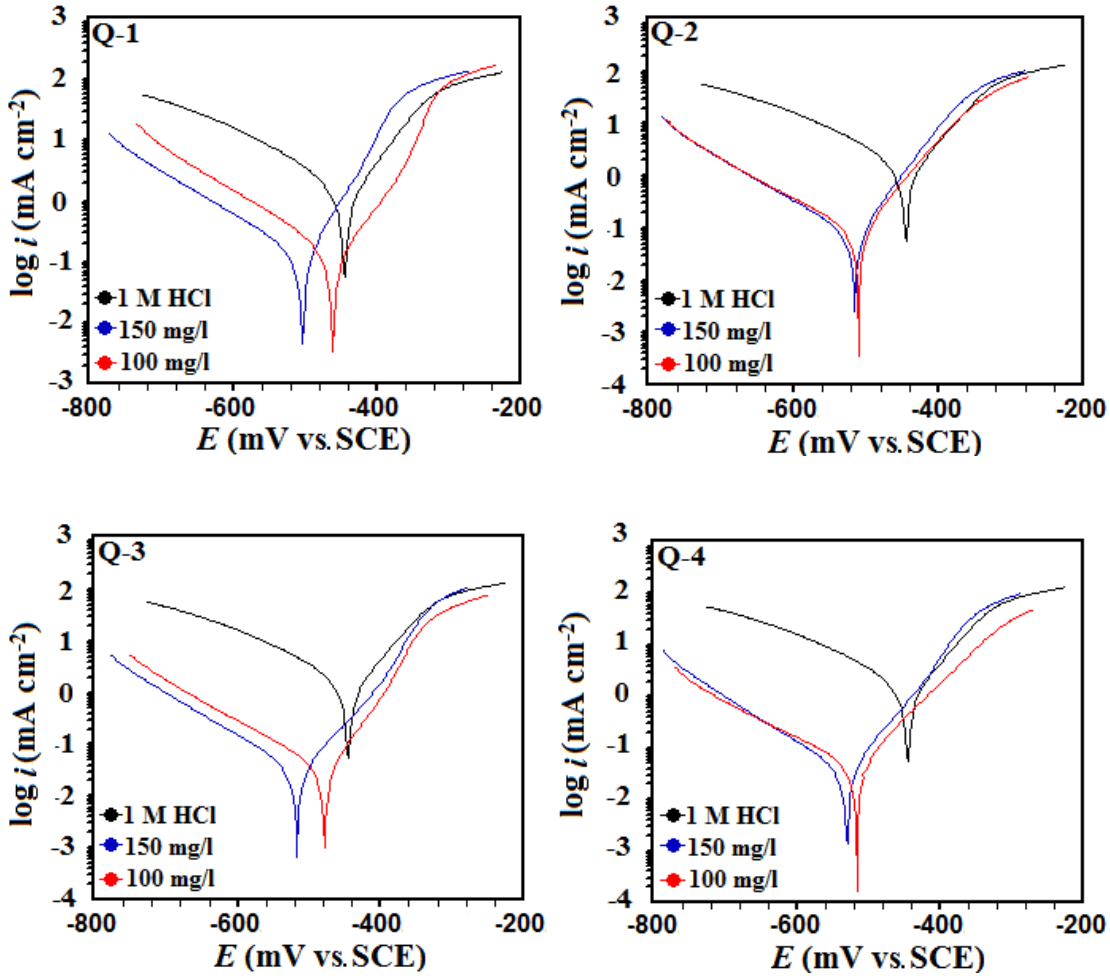

Figure 3.3.6 Polarization curves for MS in absence and presence of Quinolines in 1 M HCl.

From Figure 3.3.6, it can be seen that the addition of an inhibitor modifies both cathodic and anodic polarization branches and shifts the E_{corr} towards the negative direction as compared to an inhibitor-free solution. As previously reported in the presence of inhibitor if E_{corr} shifts more than 85 mV with respect to E_{corr} in uninhibited solution, the inhibitor can be considered as cathodic or anodic type otherwise it is of mixed type [Verma *et al.*(2014)], [Singh (2012)]. The E_{corr} values of Q-1, Q-2, Q-3, Q-4 suggested that Q-1, Q-2, Q-3 show the mixed type of inhibition with E_{corr} shift in the negative direction while Q-4 acts as a cathodic type inhibitor. The presence of all the four inhibitors causes a decrease in i_{corr} values from 182 to 36.7 μAcm^{-2}. The highest inhibition efficiency 97.35% is obtained for Q-4 at 150 mg L^{-1}.

Table 3.3.5 Polarization parameters for MS in absence and presence of Quinolines in 1 M HCl.

Inhibitors	Concentrations (mg L^{-1})	i_{corr} (µAcm-^{2})	E_{corr} (mV/SCE)	η%
Blank	0.0	1390	-445	-
Q-1	100	182	-462	86.90
	150	134	-504	90.35
Q-2	100	102	-511	92.66
	150	80.4	-516	94.21
Q-3	100	45.2	-479	96.74
	150	39.1	-517	97.18
Q-4	100	39.7	-517	97.14
	150	36.7	-531	97.35

3.3.3 Surface characterization

SEM images of the MS surface were taken to analyze the morphology before and after inhibition process. The MS sample in the absence of inhibitor shows rough and highly damaged surface due to rapid corrosion attack in acidic solution as shown in Figure 3.3.7 (a), while Figure 3.3.7 (b-e) shows a smooth and less damaged surfaces of MS in the presence of inhibitors. The protected surface obtained for MS in the presence of inhibitor suggest corrosion inhibition of MS [Verma *et al.* (2015) (c)], [Saha *et al*. (2015)]. A close examination of Figure 3.3.7 (e) reveals that the MS surface in the presence of Q-4 is the best-protected surface among all four inhibitors.

AFM analysis is further used to study surface morphology of MS surface. Figure 3.3.8 (a-e) shows the different 3D images of MS in different conditions. Figure 3.3.8 (a) shows a bumpy structure with a large number of ups and downs due to acid attack. From Figure 3.3.8 (b-e) it can be observed that on adding inhibitor in acid solution the surface morphology of MS changed and shows smoother surface suggest corrosion retardation [John and Joseph (2012)].

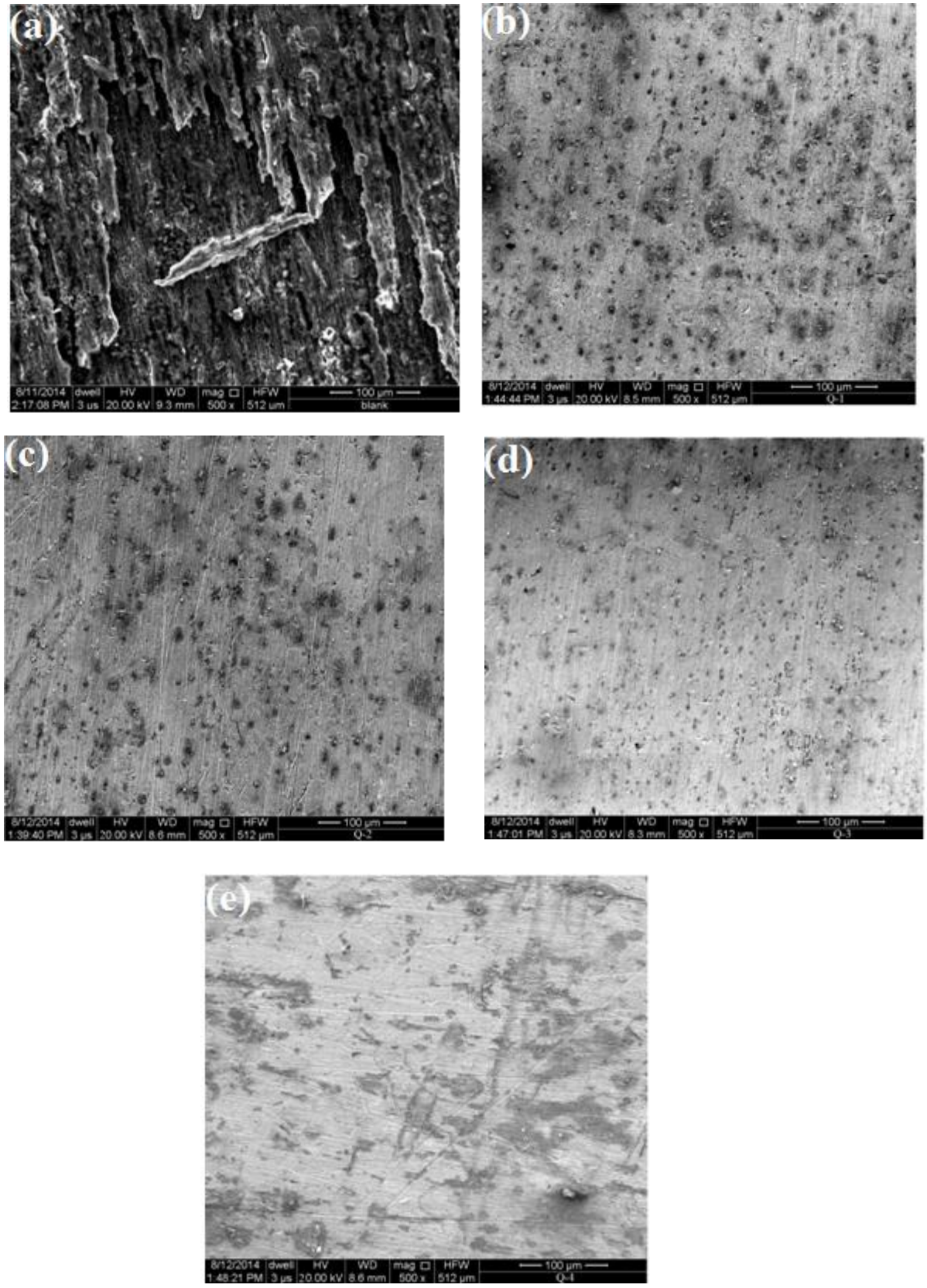

Figure 3.3.7 SEM micrographs for MS in (a) 1 M HCl and in presence of (b) Q-1 (c) Q-2, (d) Q-3, and (e) Q-4 at 150 mg L^{-1}.

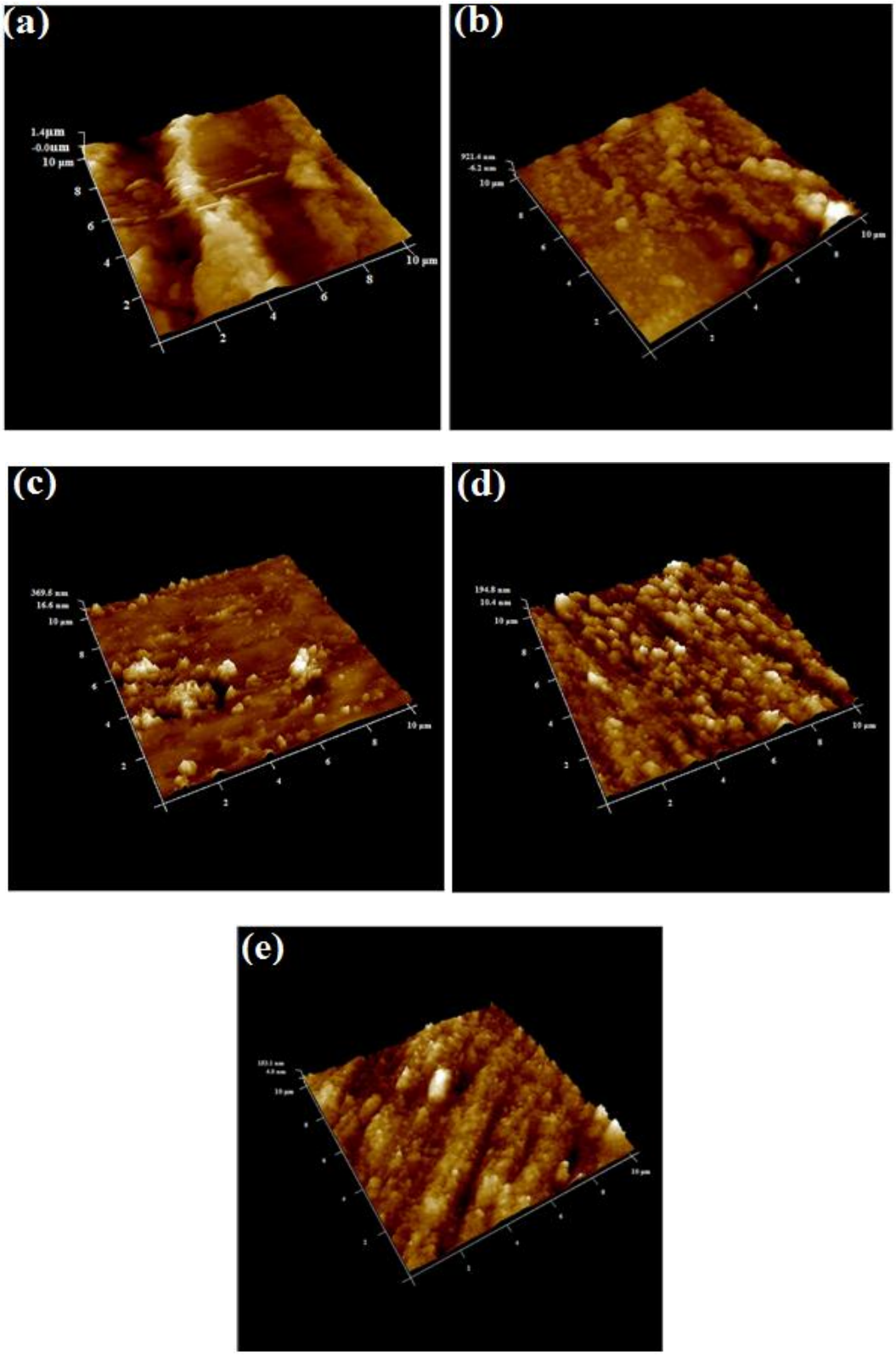

Figure 3.3.8 AFM micrographs for MS in (a) 1 M HCl and in presence of (b) Q-1 (c) Q-2, (d) Q-3, and (e) Q-4 at 150 mg L^{-1}.

The XPS analysis was used to investigate the elemental composition of adsorbed thin film of Q-4 treated MS, shown in Figure 3.3.9 (a-d). The obtained high-resolution peaks for C 1s, O 1s, N 1s and Fe 2p shows complex spectra that were analyzed through a deconvoluted fitting of complex spectra.

The deconvoluted C 1s spectrum for MS in the presence of Q-4 may be attributing to three peaks indicating three chemical forms of C atom present on the steel surface as shown in Figure 3.3.9 (a). The first peak at binding energy 285.7 eV is attributed to the C-C, C=C, and C-H of aromatic bonds. The second peak at 286.2 eV may be assigned to the carbon atom bonded to nitrogen in C-N, C=N bonds in quinoline ring. The third peak may be ascribed to the carbon atom of the C-O bond in the hydroxyl group (C–OH) at 287.0 eV [Chevalier *et al.* (2014)].

The deconvoluted O 1s spectrum may be fitted into three main peaks shown in Figure 3.3.9 (b). The first peak at 531.3 eV binding energy is attributed to O^{2-}, this could be related to oxygen atom bonded to Fe^{3+} in the FeO, Fe_2O_3, and Fe_3O_4 oxides. The second peak observed at 532.7 eV around is attributed to OH^-, which can be associated with the occurrence of hydrous iron oxides, such as FeOOH. The third peak at 533.7 eV may be assigned to the oxygen of a hydroxyl group (C–OH) in Q-4 [Boumhara *et al.* (2015)].

The deconvoluted N 1s spectrum of adsorbed thin film on MS in the presence of Q-4 may be fitted into three peaks as shown in Figure 3.3.9 (c). The first peak at 396.8 eV corresponds to C-N bonds and un-protonated N atoms in quinoline ring. The second peak at 399.4 eV is attributed to the co-ordinated nitrogen in the quinoline ring with iron (N–Fe). The last peak at 401.3 eV is attributed to positively charged nitrogen related to protonated nitrogen atom in the quinoline ring [Tang *et al.* (2013)].

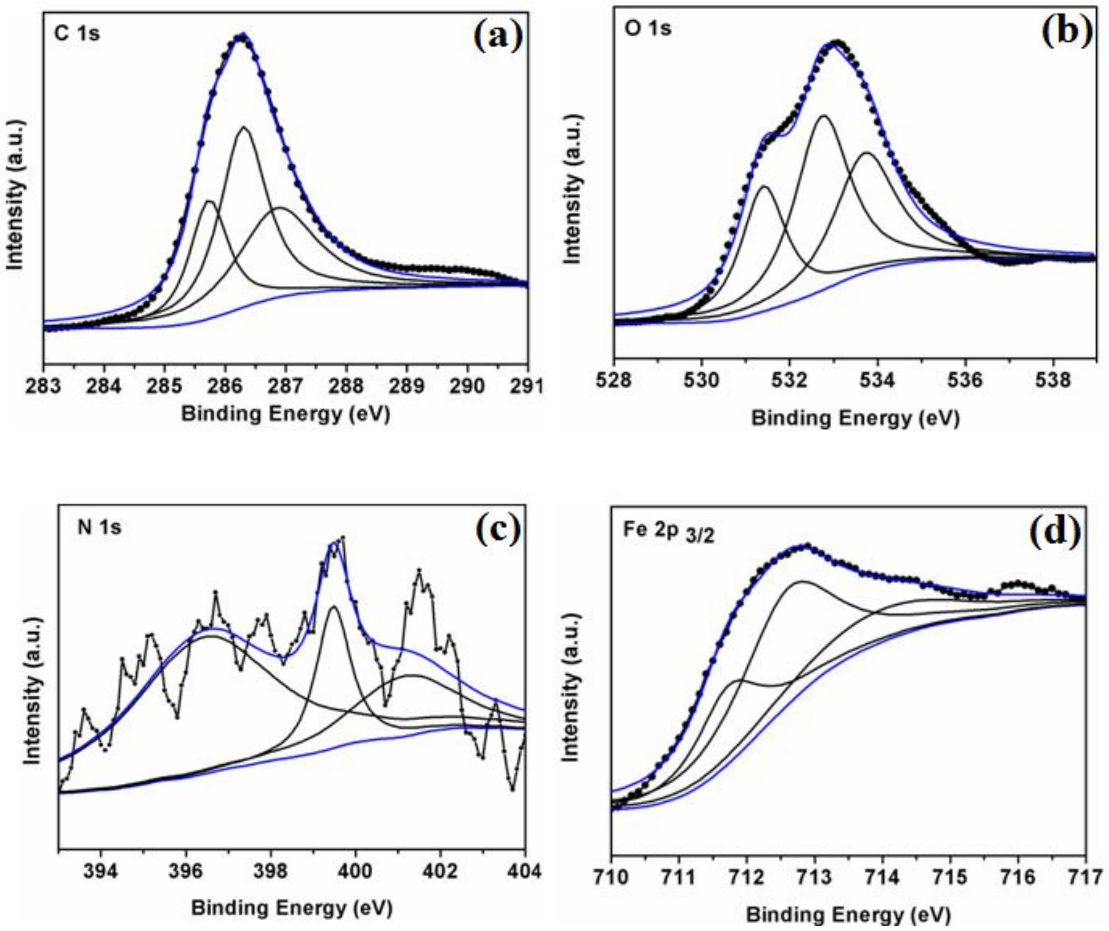

Figure 3.3.9 The XPS deconvoluted profiles of (a) C 1s, (b) O 1s, (c) N 1s, and (d) Fe $2p_{3/2}$ for Q-4 treated MS.

The deconvolution of the high peak resolution of Fe $2p_{3/2}$ spectrum consists of three peaks as shown in Figure 3.3.9 (d). The peak at 711.6 eV assigned to Fe^{3+} is attributed to ferric compounds such as Fe_2O_3 and/or FeOOH. The second peak at 712.7 eV is attributed to the presence of a small concentration of $FeCl_3$ on the MS surface. The peak at a 714.2 eV is ascribed to the satellites of Fe (III) [Tourabi *et al.* (2013)]. The results obtained by XPS analysis support the adsorption of inhibitors on MS surface.

3.4 Thiopyrimidines as corrosion inhibitors

Thiopyrimidines are important heterocyclic compounds because of their interesting pharmacological and biological activities [Criado *et al.* (2013)]. They are potential therapeutics e.g. as antiviral and anticancer [Prachayasittikul *et al*. (2011)]. There are very few reports on use of thiopyrimidine as corrosion inhibitors. Caliskan and Akbas have tested 5-benzoyl-4,6- diphenyl-1,2,3,4-tetrahydro-2-thiopyrimidin (DHPM I) as corrosion inhibitor for mild steel in 0.5 M H_2SO_4 and reported 91% inhibition efficiency at 2 x 10^{-3} M [Caliskan and Akbas (2011)]. Heterocyclic compounds containing both N and S atoms are considered as better corrosion inhibitors than those containing N and S alone [Abd El Haleem *et al.* (2013)], [Daoud *et al.* (2015)], [Yilmaz *et al.* (2016)].

Considering this, in the present work we have selected four thiopyrimidine derivatives as corrosion inhibitors for mild steel (MS) in 1 M HCl. We expected that the combined effect of both heteroatoms (N, S) present in the thiopyrimidine moiety, along with the π electrons and lone pair of electrons, better inhibitive performance could be achieved.

In present work we have synthesized four thiopyrimidine derivatives namely 5-cyano-6-phenyl-2-thioxo-2,3-dihydropyrimidin-4-one (TP-1), 5-cyano-2-thioxo-6-(p-tolyl)-2,3-dihydropyrimidin-4-one (TP-2), 5-cyano-6-(4-methoxyphenyl)-2-thioxo-2,3-dihydropyrimidin-4-one (TP-3), 6-(4-(dimethylamino)phenyl)-5-cyano-2-thioxo-2,3-dihydropyrimidin-4-one (TP-4) and evaluate their inhibiting performance on corrosion of MS with the help of different methods such as weight loss, electrochemical impedance spectroscopy (EIS), potentiodynamic polarization techniques and surface morphology by SEM /AFM/XPS.

3.4.1 Weight loss measurements

3.4.1.1 Effect of inhibitor concentration

The effect of inhibitor concentration on corrosion inhibition efficiency is shown in Figure 3.4.1 and corresponding observations are listed in Table 3.4.1.

Table 3.4.1 Weight loss measurements for MS in absence and presence of TPs in 1 M HCl at 308 K.

Inhibitors	Concentrations (mg L^{-1})	Corrosion rate (mm/y)	Surface coverage (θ)	η%
Blank	0.0	77.9	-	-
TP-1	25	48.9	0.37	37.14
	50	31.1	0.60	60.00
	75	23.7	0.69	69.52
	100	18.9	0.75	75.71
	150	11.1	0.85	85.71
	200	7.7	0.90	90.00
	250	6.3	0.91	91.90
TP-2	25	41.9	0.46	46.19
	50	26.7	0.65	65.71
	75	17.0	0.78	78.00
	100	11.1	0.85	85.71
	150	6.6	0.94	91.42
	200	4.4	0.94	94.28
	250	3.3	0.95	95.71
TP-3	25	39.7	0.49	49.04
	50	21.8	0.71	71.90
	75	13.3	0.82	82.85
	100	10.3	0.86	86.66
	150	5.1	0.93	93.33
	200	3.5	0.95	95.47
	250	2.5	0.96	96.66
TP-4	25	28.9	0.62	62.85
	50	12.2	0.84	84.28
	75	7.0	0.90	90.95
	100	4.4	0.94	94.28
	150	2.5	0.96	96.66
	200	1.8	0.97	97.61
	250	1.1	0.98	98.57

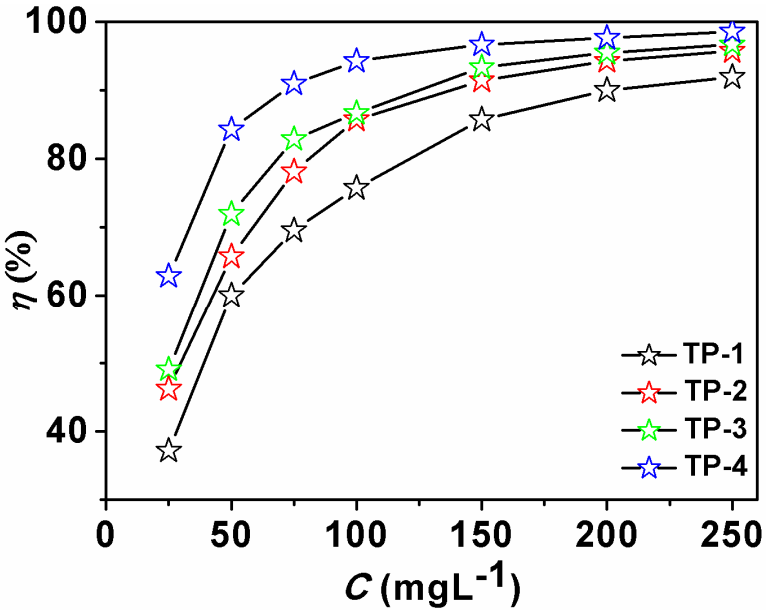

Figure 3.4.1 Effect of inhibitor concentrations (TPs) on corrosion inhibition efficiency for MS in 1 M HCl.

It can be observed that as the concentration of TPs increases (25 to 250 mgL^{-1}), the corrosion inhibition efficiency increases. This is attributed due to the adsorption of inhibitor molecules on MS surface [Dandia *et al*. (2013)], [Solomon *et al.* (2010)]. The order of inhibition efficiency is TP-4> TP-3> TP-2> TP-1. The electron donating effects of $–CH_3$, $–OCH_3$ and $–N(CH_3)_2$ groups present in TP-2 and TP-3 and TP-4 have been clearly manifested on their inhibition potentials in the study.

3.4.1.2 Effect of temperature

Temperature effect was studied in the range of 308-338K and its corresponding graph is shown in Figure 3.4.2. It can be observed from the Figure 3.4.2, as temperature increased there is decrease in the inhibition efficiency due to desorption of inhibitor molecules from MS surface.

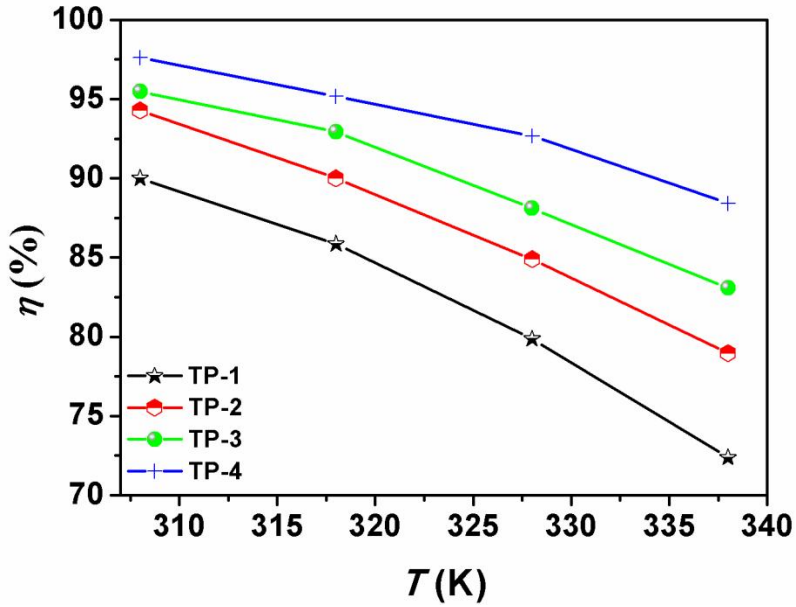

Figure 3.4.2 Effect of temperature (308-338 K) on inhibition efficiency for MS in presence of TPs in 1 M HCl

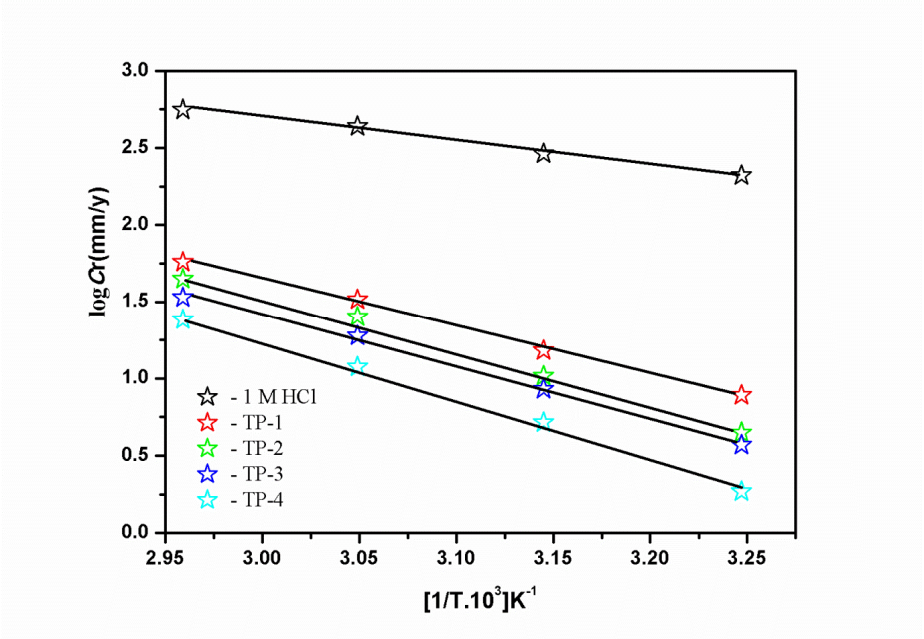

Figure 3.4.3 Arrhenius plots of log C_r vs. 1000/T for MS in 1 M HCl in the absence and presence of TPs at 200 mg L^{-1}.

In order to calculate the activation energy by Arrhenius equation, the weight loss analysis were performed in the temperature range from 308-338K at the optimum concentration of TPs.

The corrosion rate and temperature plot is shown in Figure 3.4.3 and calculated E_a values are listed in Table 3.4.2. The higher values of E_a in presence of TPs as compared in their absence reveals that the adsorption of inhibitor molecules on MS form a barrier for corrosion process [Ansari and Quraishi (2015) (b], [Zhua *et al.*(2014)], [Ansari and Quraishi (2014)], [Sudheer and Quraishi (2014)].

Table 3.4.2 Thermodynamic parameters for MS in absence and presence of TPs in 1 M HCl at 200 mg L^{-1}.

Inhibitors	***E*a (kJmol^{-1})**
Blank	29.10
TP-1	58.57
TP-2	67.62
TP-3	67.93
TP-4	73.93

3.4.1.3 Adsorption isotherm

The inhibition by TPs molecules for MS in 1 M HCl depends upon their interaction with the metal surface, which could be understood by the adsorption isotherm. In discussing the adsorption characteristics the fraction of surface coverage, θ is very useful.

The dependency of the fraction of surface covered, θ on the concentration, C of the inhibitor was tested graphically by fitting to different adsorption isotherms. Langmuir adsorption isotherm was found to be the best fitted isotherm with R^2 values very close to 1 for all TPs (Figure 3.4.4).

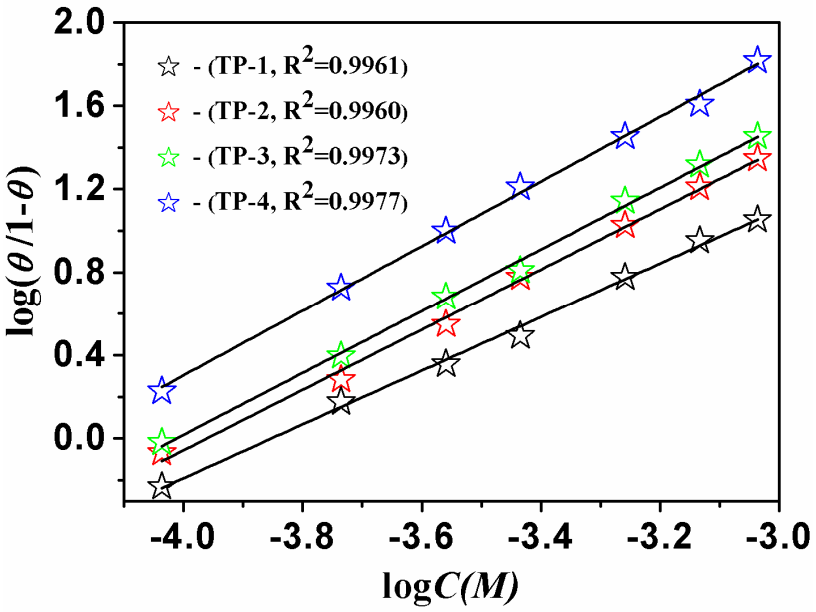

Figure 3.4.4 Langmuir adsorption isotherms for MS in presence of TPs.

Table 3.4.3 ΔG_{ads} at optimum concentration (200 mg L^{-1}) of TPs for MS in 1 M HCl at 308-338 K.

Inhibitors	Temperature	ΔG_{ads} (kJ mol^{-1})
TP-1	308	-34.39
	318	-34.29
	328	-34.25
	338	-34.22
TP-2	308	-35.91
	318	-35.51
	328	-35.16
	338	-35.13
TP-3	308	-36.53
	318	-36.16
	328	-36.07
	338	-36.03
TP-4	308	-38.26
	318	-37.49
	328	-37.30
	338	-37.17

The negative values of ΔG_{ads} suggest that adsorption of TPs are spontaneous. It is reported in the literature that if ΔG_{ads} values are in the range of -20 kJ mol^{-1} adsorption is electrostatic interaction *i.e.* physisorption, while if ΔG_{ads} values are near or greater

than -40 kJ mol^{-1} adsorption is chemisorption [R. Solmaz (2014) (a)], [Behpour *et al.* (2008)]. The ΔG_{ads} values obtained in our investigation as reported in Table 3.4.3, range from -34 to -37 kJ mol^{-1}, suggesting both physisorption and chemisorption but chemical adsorption is dominant [Khadiri *et al.* (2015)], [Guo *et al.* (2015)], [Noor El-Din and Khamis (2015)].

3.4.2 Electrochemical measurements

3.4.2.1 Electrochemical impedance spectroscopy

The Nyquist plots of MS in absence and presence of TPs are shown in the Figure 3.4.5 (a), and corresponding calculated observations are listed in Table 3.4.4.

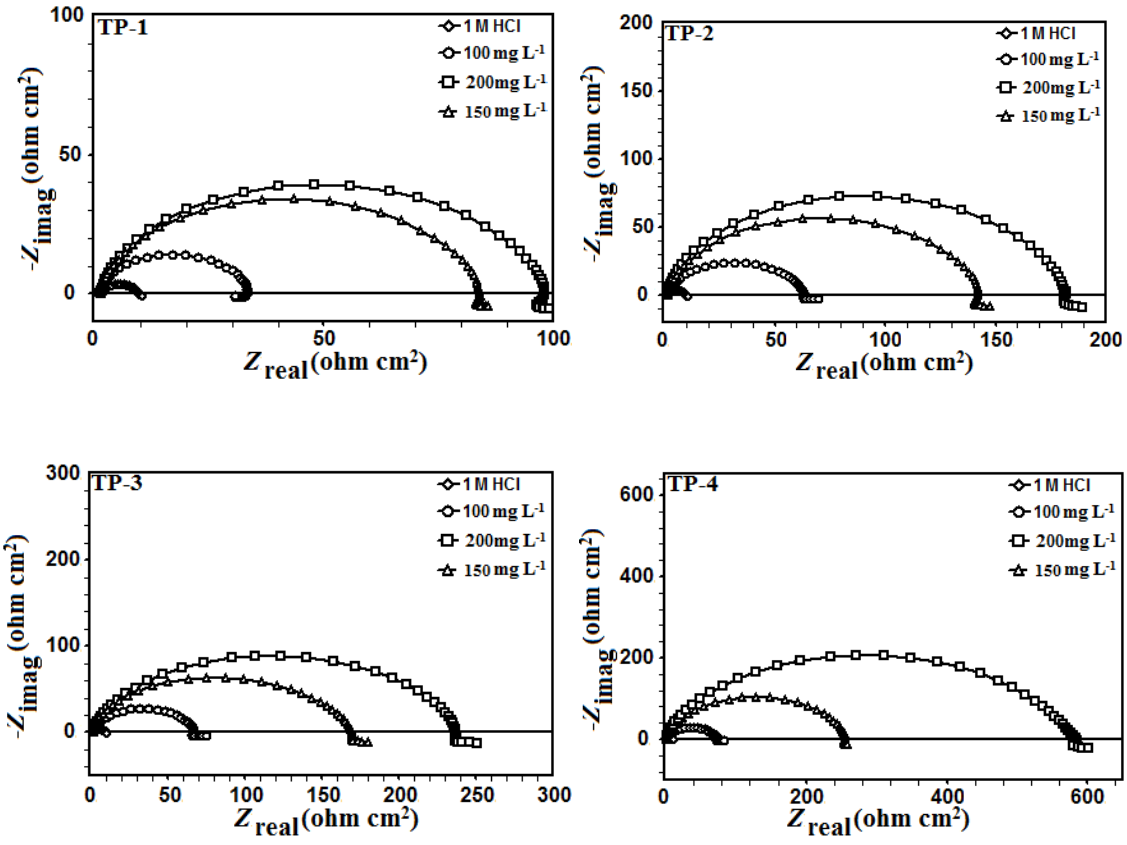

Figure 3.4.5 (a) The Nyquist plots for MS without and with TPs in 1 M HCl.

The appearance of Nyquist plots in both conditions with and without inhibitors gives a single depressed capacitive semicircle loop which indicates no change in corrosion mechanism with the addition of TPs. Also as concentration of TPs increases there is an increase in the diameter of the depressed semicircle, which confirms their inhibitory action [Bentiss *et al.* (2011)], [Juttner (1990)]. The equivalent circuit model shown in Figure 3.4.5 (b) has been used to analyze the impedance data. The values listed in Table 3.4.4 revealed that as the concentration of TPs increases there is an increase in the R_{ct} values, which suggests the adsorption of TPs over MS surface.

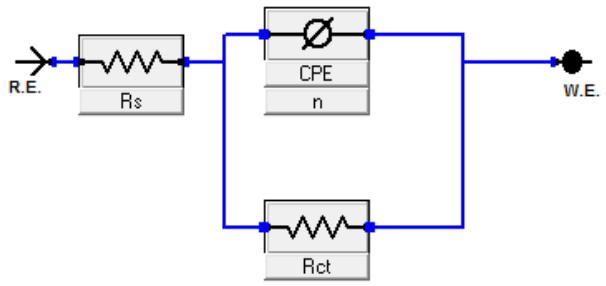

Figure 3.4.5 (b) Equivalent circuit model used to analyze the impedance data.

Table 3.4.4 Electrochemical Impedance Parameters for MS in absence and presence of TPs in 1 M HCl.

Inhibitors	**Concentrations (mg L^{-1})**	**R_{ct} (Ω cm^2)**	**C_{dl}**	**η%**	**$-S$**	**$-\alpha°$**
Blank	0.0	9.0	106	-	0.53	40.40
TP-1	100	32.3	58	72.19	0.81	65.85
	150	82.4	36	89.08	0.83	67.77
	200	95.0	26	90.52	0.84	68.38
TP-2	100	62.2	48	85.54	0.78	64.22
	150	138.7	32	93.51	0.85	69.44
	200	180.9	24	95.02	0.87	73.37
TP-3	100	66.0	39	86.38	0.85	68.07
	150	168.4	31	94.65	0.85	69.44
	200	235.6	23	96.18	0.88	73.37
TP-4	100	71.3	30	87.39	0.84	67.67
	150	252.0	22	96.42	0.87	75.76
	200	581.6	8	98.45	0.87	76.01

From Table 3.4.4 it can also observed that the values of C_{dl} decrease as the TPs concentration increases, which is attributed to a decrease in local dielectric constant or we can say increases in the thickness of electrical double layer, which suggests that the TPs are strongly adsorbed on MS surface.

Bode and phase angle plots show only one time constant (Figure 3.4.5 (c)), which is related to relaxation process corresponding to one semi-circle capacitive loop in the Nyquist plots. The ideal capacitor behaviour would result if a slope value attains -1 and phase angle values attain -90° [Sudheer and M.A. Quraishi (2013)]. In present study the Bode and phase angle values in blank are -0.53 and -40° and in presence of TPs range from -0.81 to -0.88 and -64° to -76°. This increase in slope and phase angle values as given in Table 3.4.4 suggests non-ideal behaviour of capacitor [Yadav *et al*. (2013) (a)].

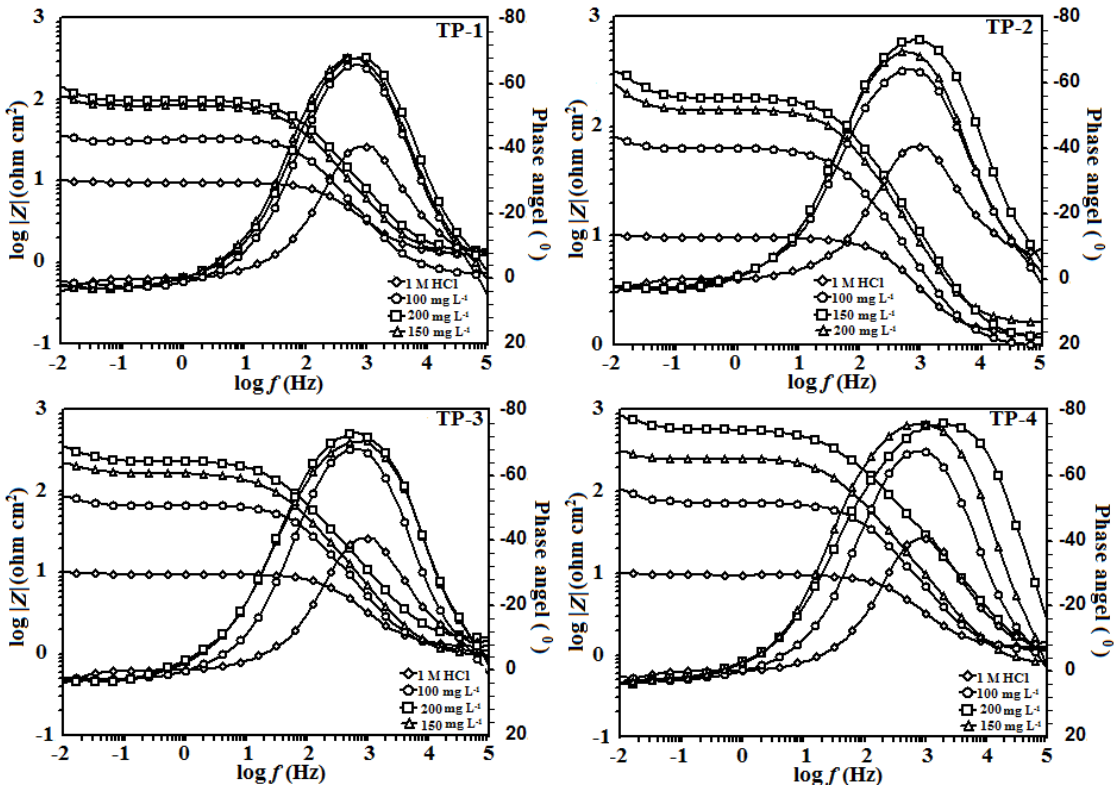

Figure 3.4.5 (c) Bode and phase angle plots for MS in 1 M HCl containing TPs.

3.4.2.2 Potentiodynamic polarization measurements

The polarization curves and related parameters for MS in absence and presence of TPs are shown in Figure 3.4.6 and obtained data is given in Table 3.4.5.

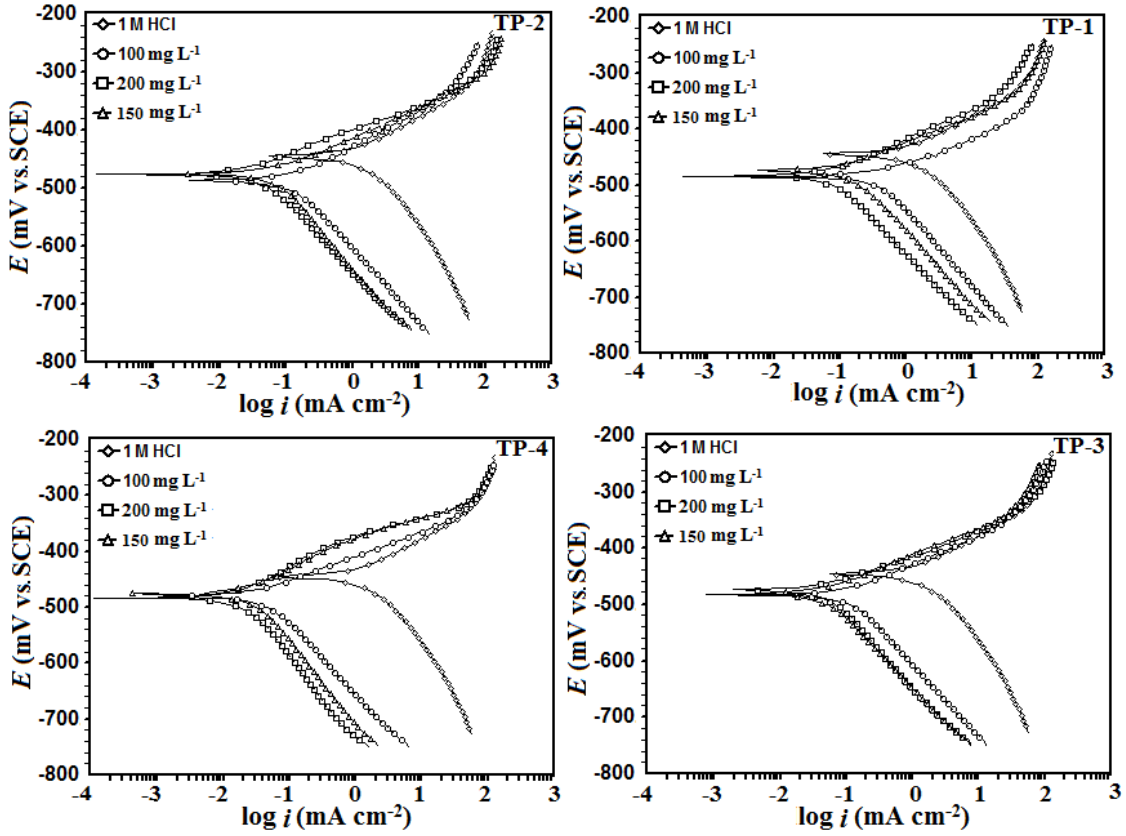

Figure 3.4.6 Polarization curves for MS in 1 M HCl containing TPs.

The shift in E_{corr} values are more towards negative side but less than 85 mV thereby suggest that TPs acts as mixed type inhibitors but predominantly inhibit cathodic reaction [Issaadi *et al*. (2011)], [Li *et al*. (2011) (b)]. The i_{corr} value in 1 M HCl is 1390 µAcm-^{2}, which is reduced in presence of inhibitors from 348 - 36.8 µAcm-^{2} at 200 mg L^{-1} confirming corrosion inhibition of MS. The inhibition efficiency follows the order TP-4>TP-3>TP-2>TP-1.

Table 3.4.5 Polarization parameters for MS in 1 M HCl containing TPs.

Inhibitors	Concentrations (mg L^{-1})	i_{corr} (µAcm-^{2})	E_{corr} (mV/SCE)	η%
Blank	0.0	1390	-445	-
TP-1	100	348	-485	74.96
	150	156	-474	88.77
	200	99.6	-483	92.83
TP-2	100	150	-487	89.20
	150	73.7	-475	94.69
	200	51.6	-486	96.28
TP-3	100	143	-482	89.71
	150	56	-481	95.97
	200	49.3	-475	96.45
TP-4	100	105	-475	92.44
	150	44.9	-476	96.76
	200	36.8	-475	97.35

3.4.3 Surface characterization

The surface morphology by SEM for MS in absence and presence of TPs at 200 mg L^{-1} are shown in Figure 3.4.7 (a-e). The rough and damaged surface of MS as shown in Figure 3.4.7 (a) is due to direct contact of MS surface with aggressive acid solution. Figure 3.4.7 (b-e) shows smooth surfaces of MS in presence of TPs suggests corrosion inhibition for MS [Singh (2012)], [Mourya *et al*. (2013)], [Verma *et al*. (2014)].

The AFM micrographs for MS in absence and presence of TPs at 200 mg L^{-1} are shown in Figure 3.4.8 (a-e). It can be seen that in absence of inhibitor the surface is highly damaged showing up and downs but in presence of TPs the image shows less damaged surface suggesting corrosion retardation [Srivastava *et al.* (2010)].

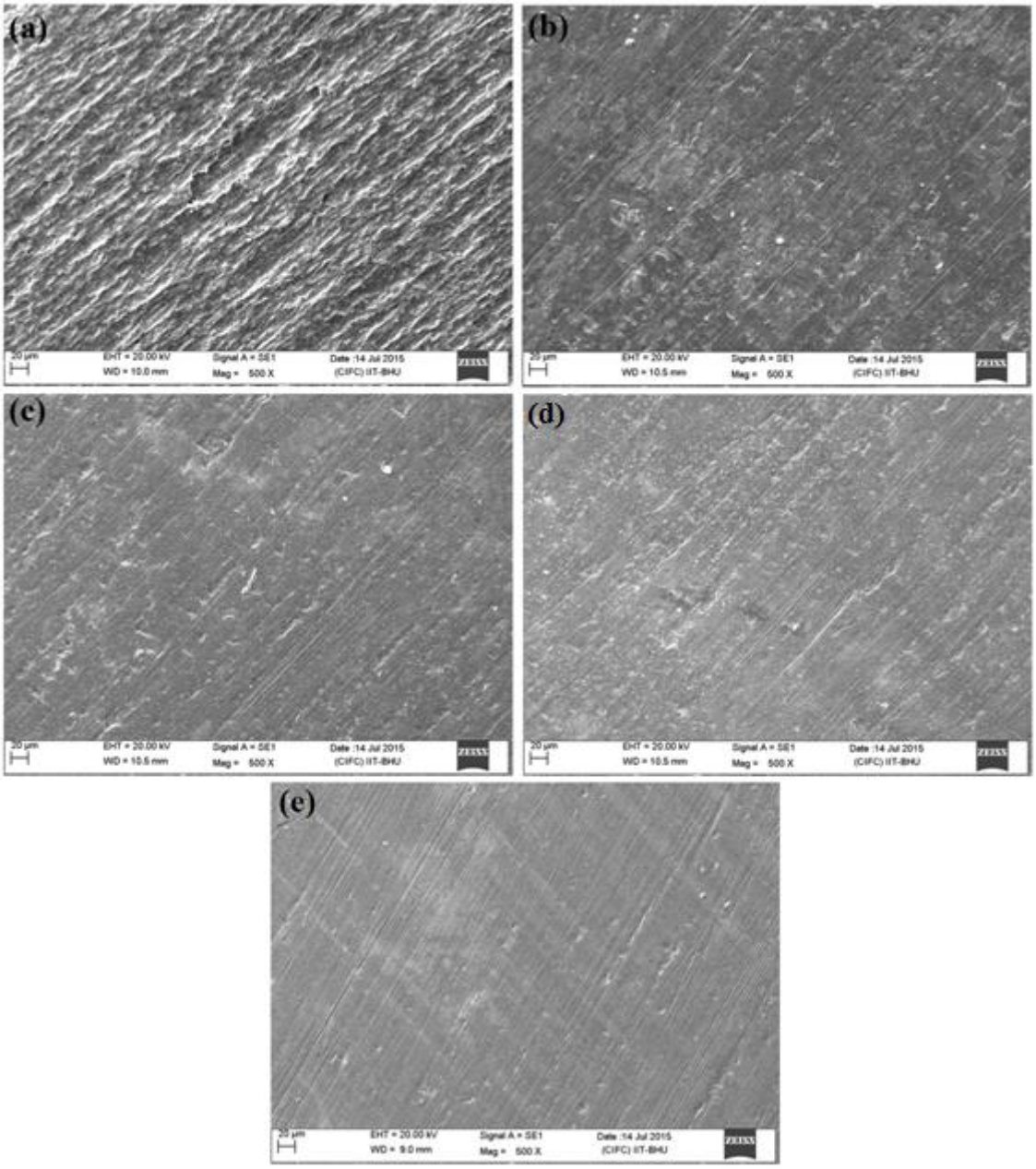

Figure 3.4.7 SEM micrographs for MS in (a) 1 M HCl and in presence of (b) TP-1 (c) TP-2 (d) TP-3 and (e) TP-4 at 200 mg L^{-1}.

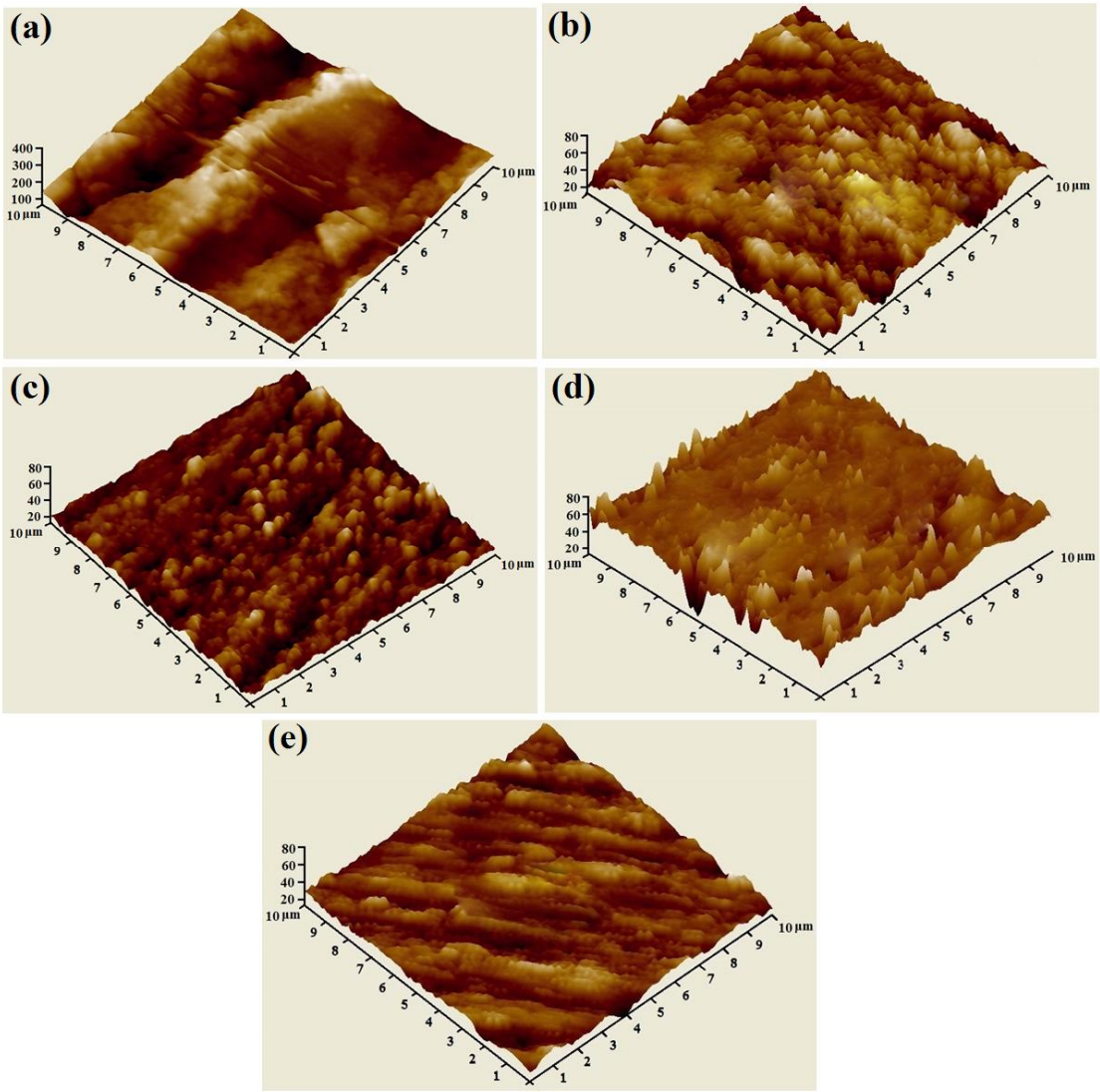

Figure 3.4.8 AFM micrographs for MS in (a) 1 M HCl and in presence of (b) TP-1 (c) TP-2 (d) TP-3 and (e) TP-4 at 200 mg L^{-1}

The XPS analysis was used to investigate the elemental composition of adsorbed thin film on MS in presence of T-4 as shown in Figure 3.4.9. The obtained high resolution peaks for C 1s, O 1s, N 1s, S 2p and Fe 2p show complex spectra which were analyzed through a deconvolution fitting procedure.

The deconvoluted C 1s spectrum for MS in presence of T-4 may attributed three peaks indicating three chemical forms of C atom present on the steel surface as shown in Figure 3.4.9 (a).

The first peak at binding energy 286.3 eV is attributed to the C-C, C=C, and C-H of aromatic bonds. The second peak at 286.9 eV may be assigned to the carbon atom bonded to nitrogen in C-N, C=N bonds in TP-4. The third peak at 287.4 eV may be ascribed to the carbon atom of the C-O bond due to carbonyl group [Bentiss *et al.* (2009)].

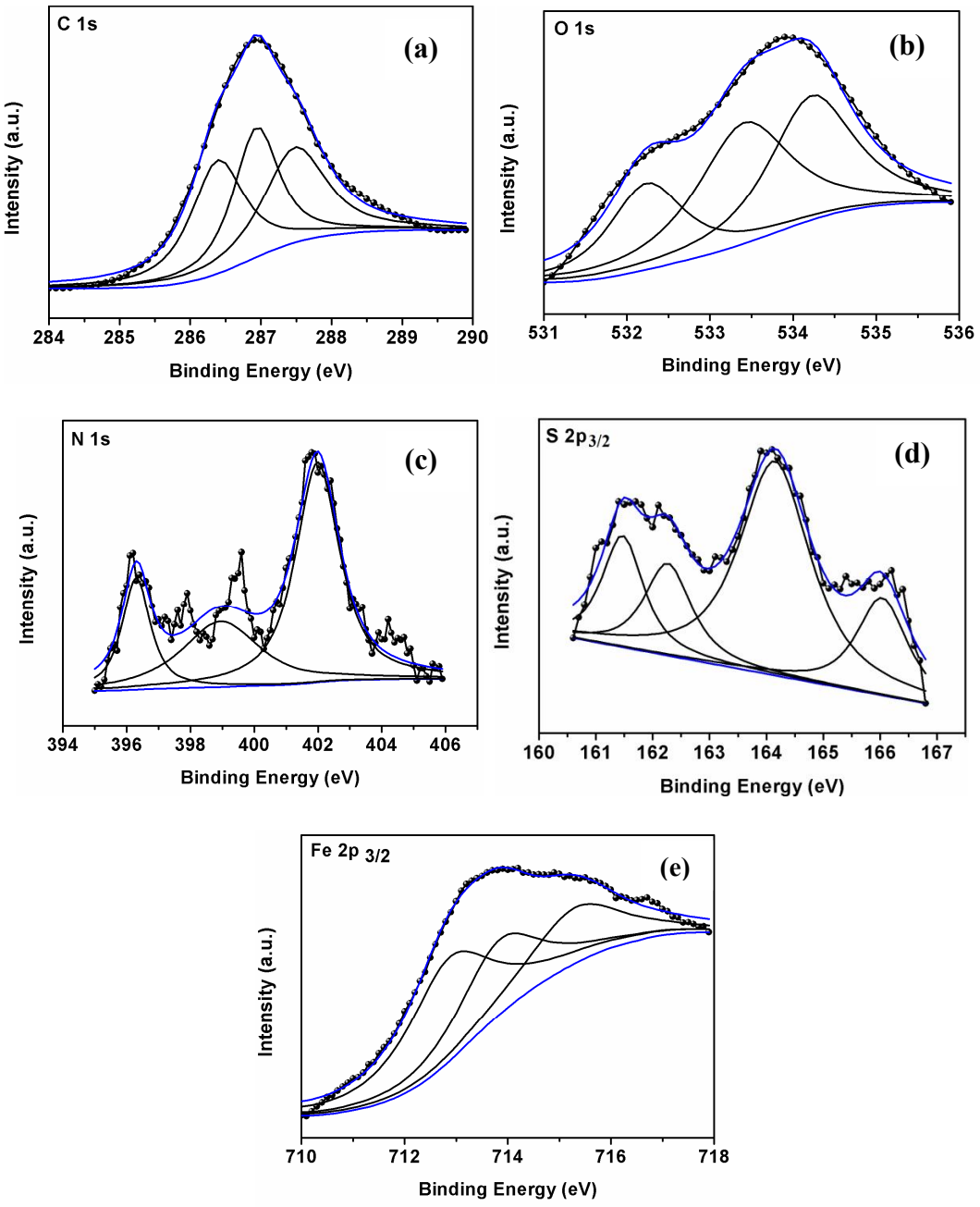

Figure 3.4.9 The XPS deconvoluted profiles of (a) C 1s, (b) O 1s, (c) N 1s, (d) S $2p_{3/2}$ and (e) Fe $2p_{3/2}$ for T-4 treated MS.

The deconvoluted O 1s spectrum for MS may be fitted into three main peaks as shown in Figure 3.4.9 (b). The first peak at 532.1 eV binding energy is attributed to O^{2-}, this could be related to oxygen atom bonded to Fe^{3+} in the FeO, Fe_2O_3 and/or Fe_3O_4 oxides. The second peak observed at 533.4 eV around is attributed to OH^-, can be associated to the presence of hydrous iron oxides, such as FeOOH. The third peak at 534.2 eV may be assigned to oxygen of carbonyl group (C–O) in T-4 and of adsorbed water [Bentiss *et al.* (2009)].

The deconvoluted N 1s spectrum of adsorbed thin film on MS in presence of T-4 may be fitted into three peaks shown in Figure 3.4.9(c). The first peak at 396.2 eV corresponds to C-N bonds and un-protonated N atoms in T-4. The second peak at 399.0 eV is attributed to the co-ordinated nitrogen in T-4 with MS (N–Fe). The last peak at 401.9 eV is attributed to positively charged nitrogen related to protonated nitrogen atom in T-4 [Tang *et al.* (2013)].

The S 2p spectrum for MS treated with T-4 shows two doublets (S $2p_{3/2}$ and S $2p_{1/2}$), with binding energy for S $2p_{3/2}$ lying at about 164.0 eV shown in Figure 3.4.9 (d). The deconvolution of high peak resolution of S $2p_{3/2}$ spectrum consists of four peaks. The first peak can be attributed to sulfide species at 161.4 eV. The second and third peak at 162.2 eV, 164 eV to neutral thiopyrimidine and last peak at 166.0 eV may assign to the S-Fe bond [Tourabi *et al*. (2013)].

The deconvolution of the high resolution peak of Fe $2p_{3/2}$ spectrum consists of three peaks shown in Figure 3.4.9 (e). The peak at 712.8 eV assigned to Fe^{3+} is attributed to ferric compounds such as Fe_2O_3 (*i.e.*, Fe^{3+} oxide), FeOOH (*i.e.*, oxyhydroxide). The second peak at 713.9 eV is attributed to the presence of a small concentration of $FeCl_3$ on the MS surface.

The peak at a 715.2 eV is ascribed to the satellites of Fe (III) [Tourabi *et al*. (2013)]. On the basis of XPS analysis, the obtained results give evidence of adsorption of inhibitor on MS surface.

3.4.4 Quantum chemical study

Quantum chemical study was performed to establish a correlation between the molecular structure of TPs and inhibition efficiency. Quantum chemical parameters such as E_{HOMO}, E_{LUMO}, ΔE, global hardness (η), softness (σ) and Mullikan charges for TPs are given in Table 3.4.6, 3.4.7.The optimized and frontier molecular orbital structures of TPs are shown in Figure 3.4.10, 3.4.11.

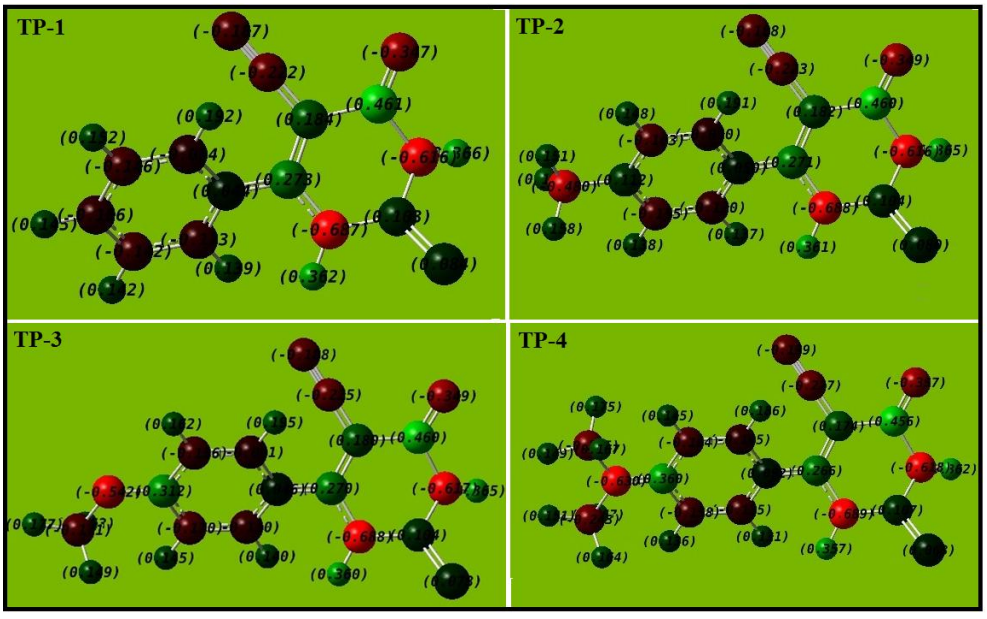

Figure 3.4.10 Optimized structures of TPs.

In general the electron donor and acceptor tendency of a molecule is given by E_{HOMO} and E_{LUMO} values. The higher the values of E_{HOMO} higher would be its electron donating ability to the metal. And higher the values of E_{LUMO} higher would be its electron accepting ability from the metal.

The energy gap, ΔE, is an important parameter which indicates the reactivity tendency of an organic molecule towards the metal surface, the lower ΔE values would cause easier electron transfer from inhibitor to metal and metal to inhibitor thereby establishing strong bond between metal and inhibitor [Hamani *et al*. (2014)].

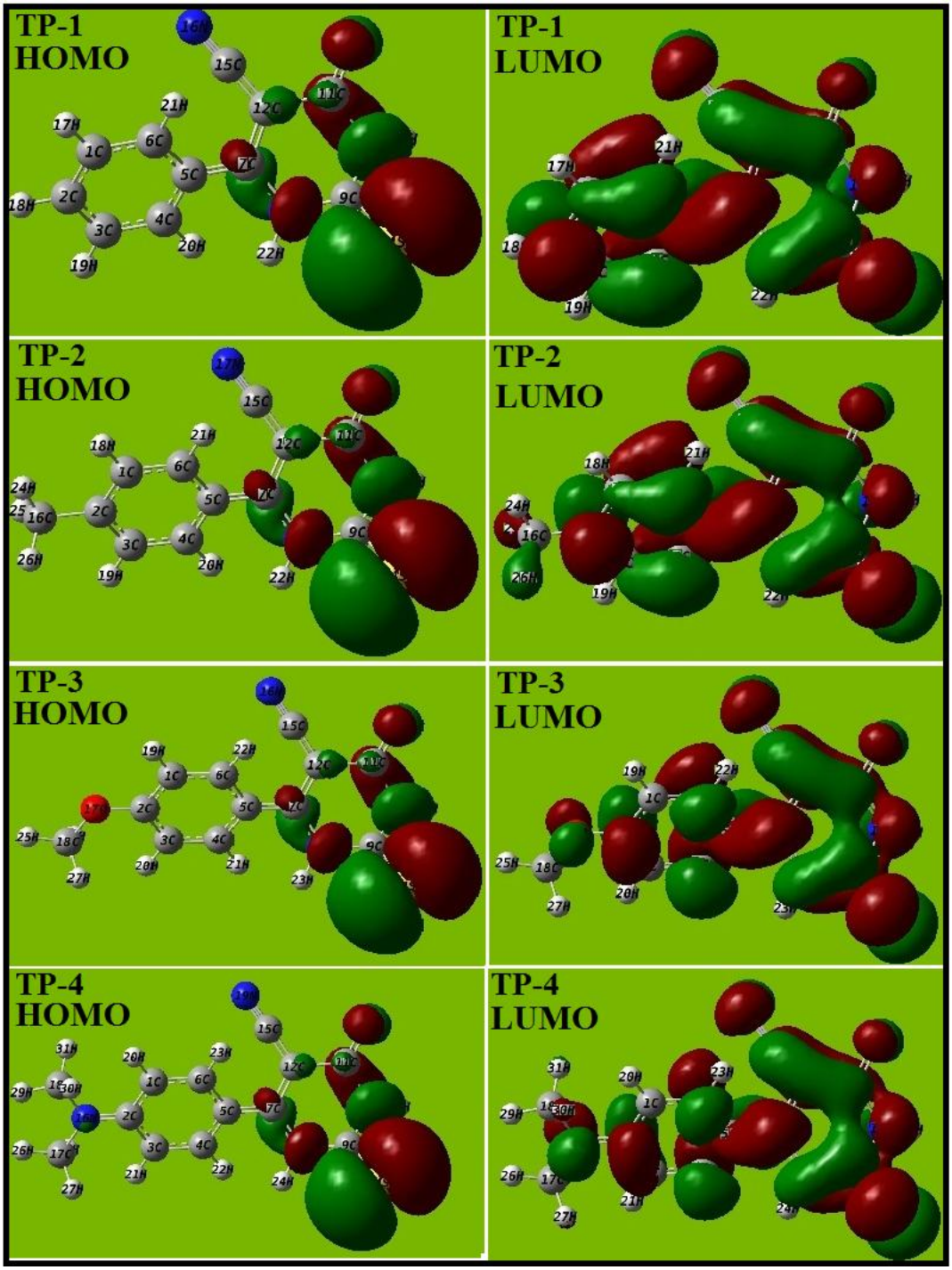

Figure 3.4.11 The frontier molecular orbital density distributions of TPs.

The parameters listed in Table 3.4.6 shows that TP-4 has highest value of E_{HOMO}, lowest value of E_{LUMO} and smallest ΔE ($\Delta E = E_{LUMO} - E_{HOMO}$) thereby suggesting that it is the best among the studied inhibitors. The order of inhibition efficiency experimentally obtained is exactly same as calculated by quantum chemical parameters.

Table 3.4.6 Calculated quantum chemical parameters for TPs.

Inhibitors	E_{HOMO} (eV)	E_{LUMO} (eV)	ΔE (eV)	η (eV)	σ (eV^{-1})
TP-1	-6.44	-2.58	3.86	1.93	0.518
TP-2	-6.34	-2.50	3.83	1.92	0.520
TP-3	-6.20	-2.47	3.72	1.86	0.537
TP-4	-5.44	-2.14	3.29	1.65	0.606

The calculated parameters like global hardness (η) and softness (σ) represents the reactivity of the molecule towards bond formation with metal [Abd El-Lateef (2015)]. According to the acid-base theory, global hardness and softness parameters are related to the description of the hard and soft acid / base [Mourya *et al*. (2015)]. A soft molecule has a small energy gap, so it can easily donate electrons to metal while a hard molecule has a large energy gap, so it requires more energy to transfer electrons to the metal. The (σ) value increases from 0.51 to 0.60 eV^{-1} for TP-1 to TP-4 and global hardness (η) decreases from 1.93 to 1.65 eV for TP-1 to TP-4.The increase in softness favours strong interaction between inhibitor and metal thereby giving high inhibition efficiency [Abd El-Lateef *et al*. (2015)]. Thus TP-4 is the softest molecule (σ =0.60 eV^{-1}) and it forms the strongest bond with metal and gives highest inhibition efficiency while TP-1 (σ =0.51eV^{-1}) shows weak interaction with metal and shows lowest inhibition efficiency.

The Mullikan charges on the heteroatoms also help to predict the possible adsorption centers. Generally more negatively charged hetero atoms are considered the most probable centers of adsorption. The results obtained show highest negative charge on the nitrogen atom on pyrimidine ring which acts as centre of adsorption. These results obtained by quantum chemical study agree well with the experimental observations.

Table 3.4.7 Mulliken charges of heteroatoms present in TPs.

Inhibitors	**Mulliken charges of heteroatoms**						
	N_1	**N_3**	**N_5**	**N_6**	**O_4**	**O_6**	**S_2**
TP-1	-0.687	-0.615	-0.186	-	-0.346	-	0.083
TP-2	-0.689	-0.621	-0.470		-0.357		0.072
TP-3	-0.689	-0.621	-0.470		-0.358	-0.543	0.070
TP-4	-0.690	-0.623	-0.630	-0.467	-0.365		0.055

3.5 General discussions for corrosion inhibition and its mechanism

Four types of heterocyclic compounds have been synthesized in the present work. The molecular structures of the heterocycles are given below:

(a) Nicotinonitriles derivatives:

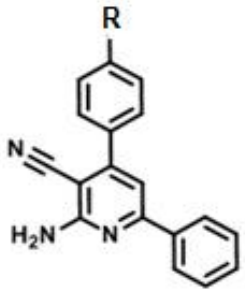

R = 1. -CH_3 (ATN), 2. -OCH_3 (AMN),

(d) Naphthyridines derivatives:

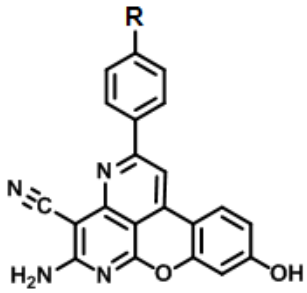

R= 3. -H (N-1), 4. -CH_3 (N-2), 5. -OCH_3 (N-3)

(c) Quinolines derivatives:

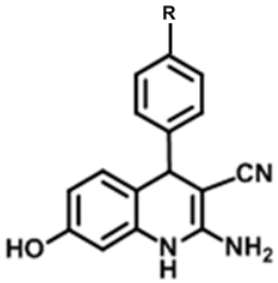

R= 6. -H (Q-1), 7. -CH_3 (Q-2), 8. -OCH_3 (Q-3), 9. -N $(CH_3)_2$(Q-4)

(d) Thiopyrimidines derivatives:

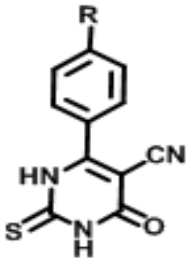

R= 10. -H (TP-1), 11. -CH_3 (TP-2) 12. -OCH_3 (TP-3), 13. -N $(CH_3)_2$(TP-4)

The inhibition efficiency of the four types of heterocyclic compounds follows the order:

Naphthyridines > **Nicotinonitriles** > **Quinolines** > **Thiopyrimidine**

Difference in inhibition efficiency

The inhibition effect of Thiopyrimidines is due to the presence of one pyrimidine ring which contains 2 N atoms, –OH, CN, and -SH as functional groups, and one substituted aromatic ring. The four Thiopyrimidines follow the inhibition order at optimum concentration of 200 mg/l, TP-1 (90.0%) < TP-2 (94.28%) < TP-3 (95.47%) <

TP-4 (97.61%). The difference in the order of the inhibition efficiency of TP-4, TP-3, TP-2 is due to the presence of electron donating groups -$N(CH_3)_2$, -OCH_3, -CH_3. TP-1 gave the lowest inhibition efficiency because it is devoid of any substituent.

The inhibition effect of Quinolines is attributed to the presence of quinoline ring attached with -NH_2, -CN and -OH functional groups along with one substituted aromatic ring. The inhibition efficiency of Quinolines at an optimum concentration of 150 mg/L follows the order: Q-1 (93.33%) < Q-2 (96.19%) < Q-3 (96.66%) < Q-4 (98.09%). The difference in the inhibition efficiency is due to the presence of different electronic donor groups. The increasing order of electron donation capabilities follows the order -$N(CH_3)_2$ > -OCH_3 > -CH_3 > -H.

The Nicotinonitriles show good inhibition performance as corrosion inhibitors due to the presence of one pyridine ring substituted with functional group -NH_2, -CN and two aromatic rings, one aromatic ring is substituted with -OCH_3, -CH_3 groups while other does not contain any substituent. The -OCH_3 substituted AMN, gave a higher inhibition efficiency of 97.14% than -CH_3 substituted ATN (95.23%) at optimum concentration 100 mg/l.

The inhibition effect of Naphthyridine derivatives is attributed to the presence of four fused aromatic rings substituted with -NH_2, -CN, -OH and one substituted aromatic ring. The inhibition order for Naphthyridines at optimum concentration of l25 mg/l is: N-3 (98.0%) >N-2 (96.6%) > N-1 (94.2%). The better performance of N-3, N-2 as compared to N-1 is ascribed to the presence of better electron donating groups -OCH_3, -CH_3 than -H.

Mechanism of Inhibition

According to the well accepted theory, the organic inhibitors are adsorbed on the metal surface by displacing water molecules [Bockris and Reddy, Modern Electrochemistry, vol. 2, (1976)].

$$Org\ (sol.) + nH_2O \rightarrow Org\ (ads) + nH_2O\ (sol.)$$

In general, owing to the complex nature of adsorption and inhibition of a given inhibitor, it is impossible to propose a single mode of adsorption between inhibitor and the metal surface. There are following possible modes through which organic inhibitor molecules can adsorb at the metal/solution interface [Li *et.al.* (2011)] in aqueous acidic solution of HCl:

(i) Electrostatic interaction of protonated inhibitor molecules with already adsorbed Cl^- ions.

(ii) Donor accepter interactions between the π-electrons of aromatic ring and the vacant d-orbitals of iron surface atoms.

(iii) Interaction between unshared electron pairs of heteroatoms and vacant d-orbitals of iron surface atoms.

(iv) Interaction of d-electrons of iron surface atoms with the vacant orbitals of hetero atoms.

In the present study four types of heterocyclic compounds have been synthesized. In these inhibitors, heteroatoms like O, N, S are present in addition to the presence of functional groups like $-NH_2$, -CN and -OH and aromatic rings consisting conjugated π electrons.

In aqueous acidic solution, the inhibitors can exist either as neutral molecules or in the form of protonated molecules which can be adsorbed on the metal surface.

$$[Inh] + xH^+ \leftrightarrow [Inhx]^{x+}$$

The mechanism of adsorption of one thiopyrimidine molecule can be represented as:

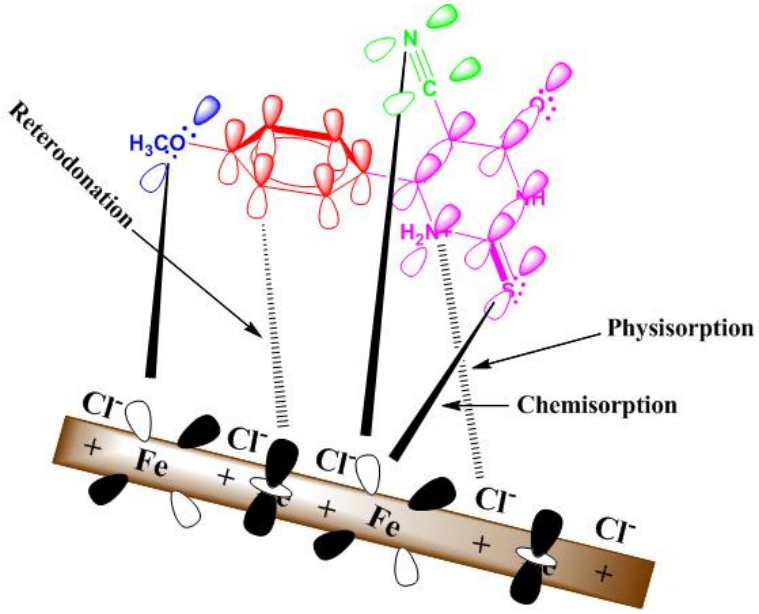

Figure 3.5.1 Pictorial representation of adsorption of TPs on MS surface in 1M HCl.

In aqueous HCl solution the thiopyrimidine molecules may adsorb through protonated heteroatoms with already adsorbed Cl^- ions on the mild steel surface. Initially, the protonated form of thiopyrimidine molecules in acid solution start competing with H^+ ions for electrons on mild steel surface. The accumulation of electrons on mild steel surface renders it more negative, and to relieve the metal from excess negative charge the electrons from the d-orbitals of Fe might get transferred to the vacant π* (anti-bonding) orbitals of thiopyrimidine molecules (reterodonation) and hence strengthen the adsorption.

It is reported that the values of ΔG^0_{ads} varying between -40 kJ mol^{-1} or more negative suggest that the adsorption is chemisorption, while the value of ΔG^0_{ads} around -20 kJ mol^{-1} or less negative implies that the adsorption is due to electrostatic interaction i.e. physisorption [Solmaz (2014) (a)]. The values of investigated inhibitors in our case ranges from -34 to -43 kJ mol^{-1} which is close to -40 kJ mol^{-1} (chemisorption). But the adsorption process cannot be solely classified as chemisorption because chemical

interactions between inhibitor molecules and metal surface are usually preceded with some form of electrostatic interactions (physisorption) as discussed. Thus there is a complex mode of adsorption of both physisorption as well as chemisorption but predominant mode is chemical adsorption [Solmaz (2014) (b)].

Life /Stability/Toxicity

These compounds are highly stable in solid state. Even after two years they have the same melting point and no change in colour has been observed. All the heterocyclic compounds investigated are known compounds; they have been synthesized by other researchers and have been found to show various biological and medicinal properties, therefore they are non-toxic.

The new inhibitors are better than already existing ones:

(a) New inhibitors exhibited more than 90% inhibition efficiency at low concentration and the best inhibitor has shown 98% inhibition efficiency at a concentration as low as 25 mg/ l.

(b) The synthetic route adopted for the preparation of heterocyclic compounds is convenient and facile. These inhibitors have been synthesized through multicomponent reactions following green chemistry principles. For this purpose the Ultrasound and Microwave techniques were utilized under mild conditions.

(c) The commercial inhibitor formulation used in industry often contains thiourea derivatives, hexamine and propargyl alcohol which are known hazardous chemicals.

Usefulness in industry: The new inhibitors can be recommended for industrial pickling process for removing rust and scales from the metal surfaces after performing preliminary tests on pilot plants.